(0, 10, 50, 100 μmol/L) for 24 or 72 h. Apoptosis was analyzed by flow cytometry using annexin V fluorescein isothiocyanate (Biolegend, San Diego, CA, USA) and propidium iodide (BD Bioscience, San Diego, CA, USA). Intracellular staining for p-ERK was performed with Ab against p-ERK purchased from R&D Systems and Alexa Flour 647 goat antirabbit immunoglobulin G (Life Technologies, Carlsbad, CA, USA) as a secondary antibody.

Statistical analysis

All experiments were repeated three times and mean ± standard deviation (SD) was shown. Statistical analysis between two groups was performed using Welch's *t*-test. $P < 0.05$ was considered statistically significant.

RESULTS

FK228 and RXM additively decreased the number of HUT-78, Ki-JK and EL-4 lymphoma cells at the doses over 50 nmol/L and 50 μmol/L, respectively (Fig. 1a). Because EL-4 cells were the most sensitive to the inhibitory effect, we used them in the following experiments. The number of EL-4 cells was significantly decreased by FK228 at 50 and 100 nmol/L (Fig. 1b). Akt phosphorylation was inhibited by FK228 at 10 and 100 nmol/L, while ERK phosphorylation was inhibited by FK228 at 100 nmol/L (Fig. 1c). Furthermore, the number of EL-4 cells was significantly decreased by RXM at 50 and 100 μmol/L (Fig. 1d). Akt phosphorylation was inhibited by RXM at 10 and 100 μmol/L, while ERK phosphorylation was inhibited by RXM at 100 μmol/L (Fig. 1e).

We have previously shown that apoptosis of EL-4 cells is inhibited by CCL11, which is dependent on ERK activation.[7] It is demonstrated that CCL27-activated CCR10-B16 melanoma cells escape apoptosis through Akt phosphorylation.[8] CCL27 induces migration of tumor cells and reactive lymphocytes into the lesional skin in CTCL.[9,10] Therefore, we next examined the effect of FK228 and RXM on EL-4 cells cultured with CCL11 and CCR10-EL-4 cells cultured with CCL27. The cell survival effect caused by CCL11 (1.0 μg/mL) was significantly inhibited by FK228 and RXM at 100 nmol/L and 100 μmol/L, respectively (Fig. 2a,b). CCL27 (100 ng/mL) did not increase the number of CCR10-EL-4 cells, although CCL27 induced Akt phosphorylation in CCR10-EL-4 cells, which was blocked by FK228 and RXM at 100 nmol/L and 100 μmol/L, respectively (Fig. 2c–f). Thus, both FK228 and RXM inhibited survival effect of CCL11, while stimulation with CCL27 and Akt phosphorylation had no effect on cell number of EL-4 cells.

To directly assess cell apoptosis, we examined EL-4 cells cultured with FK228 or RXM for 24 or 72 h by flow cytometry. Annexin V^+ EL-4 cells increased by FK228 or RXM in a dose-dependent manner (Fig. 3a–d). We next examined whether the effect of these drugs were through the inhibition of ERK phosphorylation. Annexin V^- p-ERK^+ EL-4 cells dose-dependently decreased by FK228 or RXM, while annexin V^+ p-ERK^- EL-4 cells increased (Fig. 3e–g). The frequencies of annexin V^+ cells in p-ERK^- cells were significantly higher than those of p-ERK^+ cells, suggesting that apoptosis of EL-4 cells induced by FK228 and RXM was at least partially through inhibition of ERK phosphorylation.

DISCUSSION

In this study, we demonstrated that FK228 and RXM decreased cell number of HUT-78, Ki-JK and EL-4 lymphoma cells in a dose-dependent manner. Combination of 10 or 50 nmol/L of FK228 and 10 μmol/L of RXM decreased the number of HUT78 and EL-4 cells compared to a single use of each drug (Fig. 1a). The peak plasma concentration of RXM after p.o. administration of 150 mg, a normal adult dose, is 8.1 μmol/L (6.8 μg/mL) according to the drug package insert. The concentration at 46 nmol/L (25 ng/mL) of FK228 corresponds to 50% of the free drug concentration in plasma from lung cancer patients.[11] Thus, these doses are clinically relevant in humans. The combination index analysis offers quantitative definition for additive effect (C = 1), synergism (CI < 1) and antagonism (CI > 1) in drug combinations.[12] In this study, the combination index of FK228 and RXM was almost 1, indicating that these drugs have an additive effect. Combination of two drugs may be useful to inhibit tumor growth in patients.[11,13]

We showed decrease in cell number and inhibition of ERK phosphorylation in EL-4 cells by FK228 and RXM. These drugs also blocked cell survival effect caused by CCL11, which promotes proliferation of EL-4 cells through ERK phosphorylation, but not Akt phosphorylation.[7] FK228 and RXM inhibited Akt phosphorylation at low concentrations, where they did not decrease the number of EL-4 cells. Taken together, FK228 and RXM induce apoptosis of EL-4 cells by blocking the same signaling pathway, which may be the reason why these drugs have only an additive effect rather than a synergic effect on cell survival of lymphoma cells.

In conclusion, we showed that FK228 and RXM induced apoptosis of lymphoma cells. Our *in vitro* study suggested that combination of FK228 and RXM may be helpful for enhancing tumor killing effects. Although further study is necessary, this combination may be applicable to patients with CTCL in the future.

ACKNOWLEDGMENTS: This study was supported by grants from the Ministry of Education, Culture, Sports and Technology in Japan.

CONFLICT OF INTEREST: The authors state no conflict of interest.

REFERENCES

1 Khan O, La Thangue NB. HDAC inhibitors in cancer biology: emerging mechanisms and clinical applications. *Immunol Cell Biol* 2012; **90**: 85–94.
2 Lyseng-Williamson KA, Yang LP. Romidepsin: a guide to its clinical use in cutaneous T-cell lymphoma. *Am J Clin Dermatol* 2012; **13**: 67–71.

3 Olsen EA, Kim YH, Kuzel TM *et al.* Phase IIB multicenter trial of vorinostat in patients with persistent, progressive, or treatment refractory cutaneous T-cell lymphoma. *J Clin Oncol* 2007; **25**: 3109–3115.
4 Jun YT, Kim HJ, Song MJ *et al.* In vitro effects of ciprofloxacin and roxithromycin on apoptosis of jurkat T lymphocytes. *Antimicrob Agents Chemother* 2003; **47**: 1161–1164.
5 Wakita H, Tokura Y, Furukawa F *et al.* The macrolide antibiotic, roxithromycin suppresses IFN-gamma-mediated immunological functions of cultured normal human keratinocytes. *Biol Pharm Bull* 1996; **19**: 224–227.
6 Sugaya M, Fang L, Cardones AR *et al.* Oncostatin M enhances CCL21 expression by microvascular endothelial cells and increases the efficiency of dendritic cell trafficking to lymph nodes. *J Immunol* 2006; **177**: 7665–7672.
7 Miyagaki T, Sugaya M, Murakami T *et al.* CCL11-CCR3 interactions promote survival of anaplastic large cell lymphoma cells via ERK1/2 activation. *Cancer Res* 2011; **71**: 2056–2065.
8 Murakami T, Cardones AR, Finkelstein SE *et al.* Immune evasion by murine melanoma mediated through CC chemokine receptor-10. *J Exp Med* 2003; **198**: 1337–1347.
9 Morales J, Homey B, Vicari AP *et al.* CTACK, a skin-associated chemokine that preferentially attracts skin-homing memory T cells. *Proc Natl Acad Sci* 1999; **96**: 14470–14475.
10 Kagami S, Sugaya M, Minatani Y *et al.* Elevated serum CTACK/CCL27 levels in CTCL. *J Invest Dermatol* 2006; **126**: 1189–1191.
11 Yu X, Guo ZS, Marcu MG *et al.* Modulation of p53, ErbB1, ErbB2, and Raf-1 expression in lung cancer cells by depsipeptide FR901228. *J Natl Cancer Inst* 2002; **94**: 504–513.
12 Chou TC. Drug combination studies and their synergy quantification using the Chou-Talalay method. *Cancer Res* 2010; **70**: 440–446.
13 Bryskier A. Roxithromycin: review of its antimicrobial activity. *J Antimicrob Chemother* 1998; **41**(suppl B): 1–21.

Transplantation of Engineered Chimeric Liver With Autologous Hepatocytes and Xenobiotic Scaffold

Toshiyuki Hata, MD,† Shinji Uemoto, MD, PhD,* Yasuhiro Fujimoto, MD, PhD,* Takashi Murakami, MD, PhD,‡ Chise Tateno, PhD,§ Katsutoshi Yoshizato, PhD,§ and Eiji Kobayashi, MD, PhD||*

Objective: Generation of human livers in pigs might improve the serious shortage of grafts for human liver transplantation, and enable liver transplantation without the need for deceased or living donors. We developed a chimeric liver (CL) by repopulation of rat hepatocytes in a mouse and successfully transplanted it into a rat recipient with vessel reconstruction. This study was designed to investigate the feasibility of CL for supporting the recipient after auxiliary liver grafting.

Methods: Hepatocytes from luciferase transgenic or luciferase/LacZ double-transgenic rats were transplanted into 20- to 30-day-old urokinase-type plasminogen activator/severe-combined immunodeficiency (uPA/SCID) mice (n = 40) to create CLs with rat-origin hepatocytes. After replacement of mouse hepatocytes with those from rats, the CLs were transplanted into wild-type Lewis (n = 30) and analbuminemia (n = 10) rats, followed by immunosuppression using tacrolimus (TAC) with/without cyclophosphamide (CPA) or no immunosuppression. Organ viability was traced by in vivo bioimaging and Doppler ultrasonography in the recipient rats for 4 to 6 months. Rat albumin production was also evaluated in the analbuminemia rats for 4 months. In addition, histological analyses including Ki67 proliferation staining were performed in some recipients.

Results: Both immunosuppressive protocols significantly improved graft survival and histological rejection of CLs as compared to the nonimmunosuppressed group. Although rat albumin production was maintained in the recipients for 4 months after transplantation, ultrasonography revealed patent circulation in the grafts for 6 months. Ki67 staining analysis also revealed the regenerative potential of CLs after a hepatectomy of the host native liver, whereas immune reactions still remained in the mouse-origin structures.

Conclusions: This is the first report showing that engineered CLs have potential as alternative grafts to replace the use of grafts from human donors.

Keywords: alternative organ graft, auxiliary liver transplantation, chimeric liver, engineered organ, liver transplantation

(*Ann Surg* 2013;257: 542–547)

From the *Division of Hepato-Biliary-Pancreatic and Transplant Surgery, Department of Surgery, Graduate School of Medicine, Kyoto University, Kyoto, Japan; †Division of Transplantation Surgery, Mayo Clinic Florida, Jacksonville; ‡Department of Pharmacy, Takasaki University of Health and Welfare, Gunma, Japan; §PhoenixBio Co Ltd, Higashi-Hiroshima, Japan; and ||Division of Development of Advanced Treatment, Center for Development of Advanced Medical Technology, Jichi Medical University, Tochigi, Japan.

Disclosure: Supported by a Grant-in-Aid for Scientific Research (No 20249058) from the Japan Society for the Promotion of Science, the "Strategic Research Platform" for Private Universities, a matching fund subsidy from the Ministry of Education, Culture, Sports, Science and Technology of Japan (2008), the COE program from MEXT (2008), and the Kyoto University Foundation (2011). E.K. is a chief scientific advisor for Otsuka Pharmaceutical Factory, Inc. This work was not supported by any funding from the National Institute of Health, Wellcome Trust, or Howard Hughes Medical Institute.

Supplemental digital content is available for this article. Direct URL citations appear in the printed text and are provided in the HTML and PDF versions of this article on the journal's Web site (www.annalsofsurgery.com).

Reprints: Eiji Kobayashi, MD, PhD, 3311-1 Yakushiji, Shimotsuke, Tochigi 329-0498, Japan.E-mail: eijikoba@jichi.ac.jp.

ISSN: 0003-4932/13/25703-0542
DOI: 10.1097/SLA.0b013e31825c5349

Liver transplantation is currently regarded as the most effective treatment for end-stage liver diseases. Because the worldwide graft shortage remains unresolved,[1,2] engineered organs are anticipated as alternative grafts to fill the scarcity and ultimately replace those from deceased and living donors. Although regenerative technology has already developed various kinds of regenerative cells and tissues,[3,4] they are still insufficient to cure patients with end-stage liver diseases because of the absence of complicated functions and limited volume. Therefore, a regenerative liver graft for use as an "organ" is required. To achieve an appropriate 3-dimensional structure and differentiation to specific tissues in a single organ, application of native organs as scaffolds has been reported as a possible solution.[5–7] Recent advances in genetic manipulation of animals such as pigs have produced transgenic animals with a lower risk of xenorejection.[8,9] Thus, using their native organogenetic potentials, development of engineered liver "organs" is expected.[10] In such a protocol, human hepatocytes are transplanted to a transgenic pig to replace its native hepatocytes, resulting in development of a chimeric liver (CL) with human parenchyma and swine nonparenchymal components, including vessels, bile ducts, and other connecting tissues. However, it is unclear whether such engineered CLs can be transplanted into recipients, or whether they can maintain their organ structures and functions after transplantation. In this study, we developed a rodent model of chimeric liver transplantation to investigate its feasibility (Fig. 1A). We used mice and rats as substitutes for transgenic pigs and humans, respectively, and created CLs in transgenic mice using hepatocytes derived from transgenic rats. After chimeric liver transplantation into rat recipients with vessel reconstruction, we examined the long-term viability and functions of the transplanted CL grafts.

MATERIALS AND METHODS

Animals

All mice and rats were housed in a temperature-controlled environment under a 12-hour light-dark cycle with free access to water and standard rodent chow diet. Male and female albumin enhancer-/promoter-driven urokinase-type plasminogen activator/severe-combined immunodeficiency (uPA/SCID) mice (Phoenixbio Co, Ltd, Japan) (n = 40), which express and accumulate urokinase-type plasminogen specifically in native hepatocytes, resulting in liver disease,[11,12] were used as the scaffolds for CL regeneration. Male luciferase transgenic Lewis (Luc-LEW) (MHC haplotype; $RT1^l$)[13] (n = 2), and female luciferase and LacZ double-transgenic Lewis (Luc/LacZ-LEW) ($RT1^l$) rats[14] (n = 1) were used as hepatocyte donors. Male wild-LEW rats ($RT1^l$) (Charles River Japan, Japan) (n = 30) and male Nagase analbuminemia rats ($RT1^a$)[15] (Japan SLC, Japan) (n = 10) were used as the recipients of chimeric liver transplantation. All experiments in this study were performed in accordance with the Jichi Medical University Guide for Laboratory Animals after approval by the ethics committee of PhoenixBio Co, Ltd.

Generation of CLs

Isolated hepatocytes were obtained from 10-week-old Luc-LEW and Luc/LacZ LEW rats using a standard 2-step collagenase

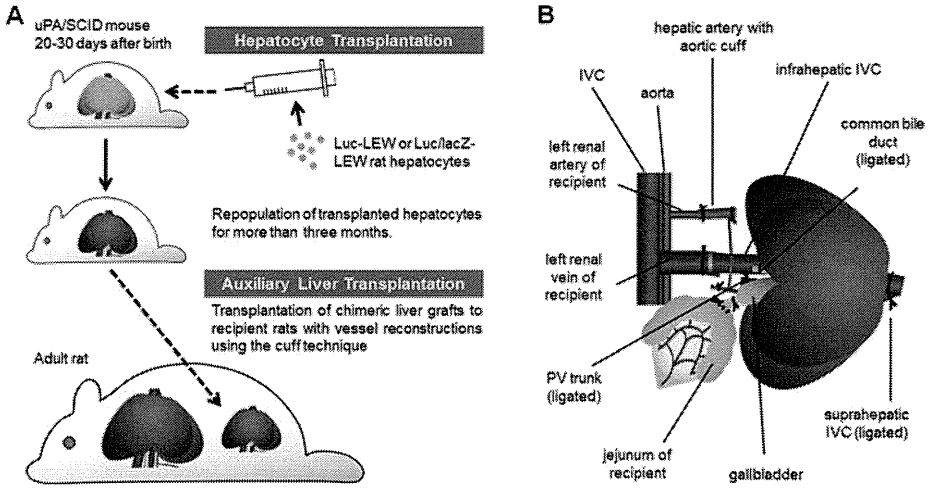

FIGURE 1. A, Experimental protocol used for Chimeric liver transplantation. B, Schema of engraftment of CL into recipient rat.

perfusion method.[16] Collagenase (75 mg/body) (COLLAGENASE S-1; Nitta-gelatin, Japan) was perfused through the portal vein, then 5.0 $\times$ 10^5 hepatocytes were transplanted into 20- to 30-day-old uPA/SCID mice, as previously reported.[12] These mice were kept for 3 months to obtain CLs with satisfactory size (mean $\pm$ SEM, 1.69 $\pm$ 0.04 g) and chimerism.

Harvesting of CLs

The CLs were harvested from uPA/SCID mice along with the hepatic artery with the aortic cuff and infrahepatic inferior vena cava. The portal vein trunk, common bile duct, and suprahepatic inferior vena cava were ligated. After systemic injection of 300 U of heparin sodium (Novo-Heparin; Mochida, Japan), the graft was harvested and cryo-preserved in 0.9% saline. A 10-mm plastic tube (22G SurfloR, IV catheter; Terumo, Japan) was inserted into the gallbladder, and a plastic cuff (18G SurfloR) was installed onto the end of the infrahepatic inferior vena cava.

Auxiliary Liver Transplantation of CLs

The CLs were engrafted in an auxiliary manner with vessel reconstruction using a cuff technique, as we previously reported.[17] In brief, after a simple left nephrectomy, a plastic cuff (22G SurfloR) was installed on the end of the recipient left renal artery. The graft hepatic artery and infrahepatic inferior vena cava were anastomosed to the recipient left renal artery and vein, respectively (see Video and Figure, Supplemental Digital Contents 1 and 2, demonstrating reperfusion of graft, available at http://links.lww.com/SLA/A254 and http://links.lww.com/SLA/A256, respectively). The graft gallbladder was connected to the recipient jejunum (Fig. 1B) and the recipient liver was left intact. There were no significant differences regarding any of the parameters for the animals and surgical procedures (data not shown). Recipient rats that died within 24 hours after chimeric liver transplantation or showed no luminescent signals on day 1 were excluded from postoperative analyses.

PostTransplant Treatment

Solid immunosuppressive protocols with tacrolimus (TAC) for T cell-mediated rejection and cyclophosphamide (CPA) for antibody-mediated rejection were used. The LEW rat recipients were treated with one of the following protocols: daily tacrolimus [TAC (+)CPA (−)] (n = 15), daily tacrolimus and cyclophosphamide pretreatment [TAC (+)CPA(+)] (n = 6), or no immunosuppression [TAC(−)CPA(−)] (n = 6). In the TAC(+)CPA(−) and TAC(+)CPA(+) groups, tacrolimus (Prograf; Astellas, Japan) was injected intramuscularly into the recipient rats at a dose of 0.64 mg/kg before and every day after transplantation. In TAC (+)CPA(+), candidate recipient rats were prepared with an intraperitoneal injection of cyclophosphamide (Endoxan, Shionogi, Japan) at a dose of 60 mg/kg 10 days before transplantation (dose of cyclophosphamide modified from previous report[18]). For Nagase analbuminemia rat recipients (n = 8), tacrolimus was given every day intramuscularly at a dose of 0.32 mg/kg. The recipient rats were observed daily and those in very poor condition were euthanized.

Evaluation of Luminescence From CLs

In vivo luciferase imaging of CLs was performed in both uPA/SCID mice for 3 months after hepatocyte transplantation and recipient rats throughout their survival after chimeric liver transplantation using a noninvasive bioimaging system (IVIS, Xenogen, CA), and the images were analyzed using a software package (Igor; WaveMetrics, OR, and IVIS Living Image; Xenogen). Before imaging, D-luciferin (potassium salt; Biosynth, Switzerland) (30 mg/kg) was injected into the peritoneal cavity of uPA/SCID mice or the penile vein of recipient rats. Signal intensity was quantified as photon flux in units of photons (s/cm^2/steradian) in the region of interest.

ELISA for Serum Rat Albumin Levels

Blood samples were obtained from uPA/SCID mice for 3 months after hepatocyte transplantation and Nagase analbuminemia rat recipients for 4 months after chimeric liver transplantation. To examine hepatic functions specific to CLs in our model with an intact recipient liver, we measured serum rat albumin using a Rat Albumin ELISA KIT (AKRAL-120, Shibayagi, Japan).

Histological Analyses

Tissue samples were fixed in 10% formalin for hematoxylin-eosin staining, and 10-μm thick sections were used. For X-gal and immunohistochemical staining, 4%-paraformaldehyde-fixed frozen samples were sliced into 4-μm thick sections. X-gal analyses were performed as previously reported.[14] Immunohistochemical analyses of the CL grafts were performed before and 2 days after the host left lobectomy with anti-Ki67 rabbit polyclonal antibody (RB-1510-P, Thermo Fisher Scientific, CA). Fifteen random views of each sample were obtained and Ki67-positive hepatocytes were separately counted in areas (mm^2) with viable hepatocytes using image software (Scion Image; Scion, MD).

Ultrasonographic Analyses

Blood flow velocities were measured using an ultrasound system (Prosound SSD-α5; ALOKA, Japan). Velocity was quantified in unit of cm/second.

Statistical Analyses

We performed statistical analyses using StatView5.0 (SAS, NC). We used the analysis of variance test and Holm-Sidak as a post hoc test. Data are presented as the mean ± SEM, with values of $P < 0.05$ considered to be statistically significant.

RESULTS

Development of CL Grafts in Mice

On the basis of the repopulation of transplanted rat hepatocytes in uPA/SCID mice, the spreading of positive areas was observed using in vivo bioluminescent imaging (Fig. 2A). Luminescent fluxes increased rapidly and reached a plateau for approximately 3 months after hepatocyte transplantation (Fig. 2B). Moreover, serum rat albumin concentration on day 30 was significantly higher than that on day 5, then remained until day 85 (Fig. 2C). Luminescent fluxes and albumin concentrations were strongly correlated (Spearman correlation coefficient $r = 0.86$, $P < 0.0001$), suggesting that luminescence reflected CL function. The appearance was that of a normal mouse liver (Fig. 2D). Although hematoxylin-eosin staining showed normal histological structures, X-gal staining revealed that the mouse hepatic parenchyma was nearly entirely replaced by LacZ-positive rat hepatocytes, except for the other hepatic components, such as the vessels and bile ducts in Glisson capsules (Fig. 2E).

Graft Viability After Auxiliary Transplantation

In the TAC(−)CPA(−) group, luminescence vanished rapidly until day 5 after Chimeric liver transplantation, whereas it was stably maintained for 4 weeks in both TAC(+)CPA(−) and TAC(+)CPA(+). There was no significant difference between those 2 groups (Fig. 3A).

Histological Analyses of Transplanted CL Grafts

Hematoxylin-eosin staining showed massive necrosis and destruction of the arrangement of the hepatic lobules in TAC(−)CPA(−) on day 5 (Fig. 3B). In contrast, TAC(+)CPA(−) on day 7 showed maintenance of those, even with massive cellular infiltration from the Glisson capsules to the central areas (Fig. 3C). Furthermore, in TAC(+)CPA(+), the hepatic structures were maintained with fewer rejection changes (Fig. 3D). Even on day 14, the TAC(+)CPA(+) protocol protected the CL from severe xenobiotic rejection, with only moderate cellular infiltration in the Glisson capsules (Fig. 3E).

Long-Term Patency of Reconstructed Vessel Circulations

Doppler ultrasonography showed the flow patterns of the arterial inflow and venous outflow in the transplanted CLs on days 14 and 188 in the TAC(+)CPA(−) group. Peak velocities on day 14 were 34.2 (artery) and 9.9 (vein) cm/s, whereas those on day 188 were 12.5 and 3.4 cm/s, respectively (See Figure, Supplemental Digital Content 3, available at http://links.lww.com/SLA/A257).

Long-Term Maintenance of Secretion of Rat Albumin in Nagase Analbuminemia Rats

Although serum rat albumin concentrations in Nagase analbuminemia rat recipients were undetectable before Chimeric liver transplantation, the transplanted CLs produced albumin on day 5 and then maintained production for 4 months, with maintenance of luminescence under the TAC(+)CPA(−) protocol (Fig. 4A).

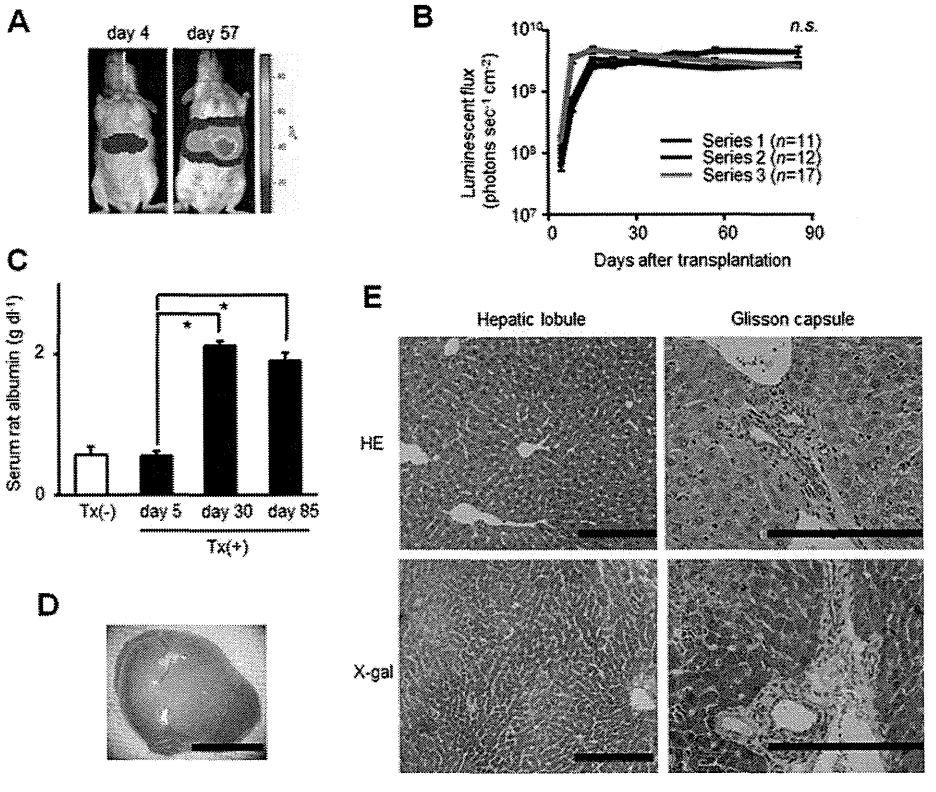

FIGURE 2. Development of CL grafts in uPA/SCID mice. A, Spread of luminescence-positive area. B, Luminescence after hepatocyte transplantation in 3 independent series. *n* as indicated; values are shown as the mean ± SEM; *n.s.*, no significant difference on day 85. C, Production of rat albumin by transplanted rat hepatocytes in mice ($n = 12$). *P <0.01; Values are shown as the mean ± SEM; Tx, hepatocyte transplantation. D, Macroscopic appearance of CL before engraftment. Scale bar = 10 mm. E, hematoxylin-eosin and X-gal staining of intact CLs. The results shown are representative of 5 separate analyses. Scale bars = 200 μm.

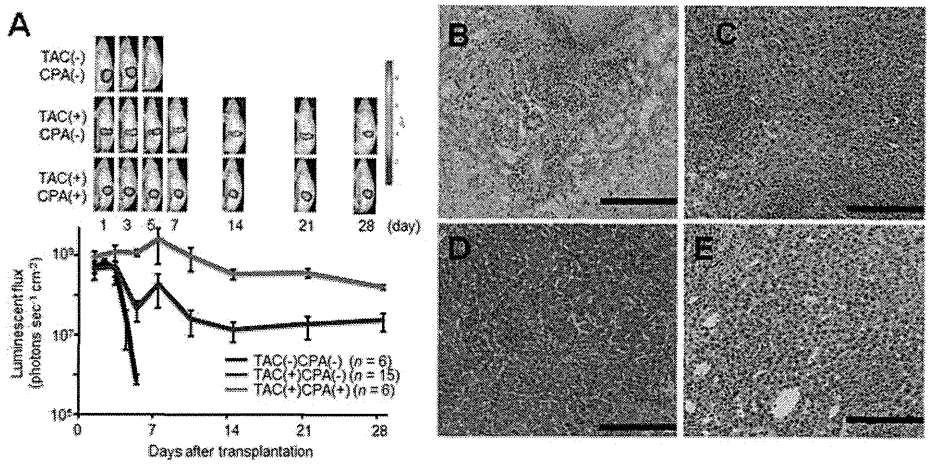

FIGURE 3. Viability of transplanted CL grafts in wild-type LEW rat recipients. A, Luminescence from transplanted CLs. Each in vivo luminescent image is representative of 3 independent groups. *n* as indicated. B–E, Histological analyses of transplanted CLs. The figures present independent recipients. B, Graft with TAC(−)CPA(−) on day 5. C, Graft with TAC(+)CPA(−) on day 7. D, Graft with TAC(+)CPA(+) on day 4. E, Graft with TAC(+)CPA(+) on day 14. Scale bars = 200 μm.

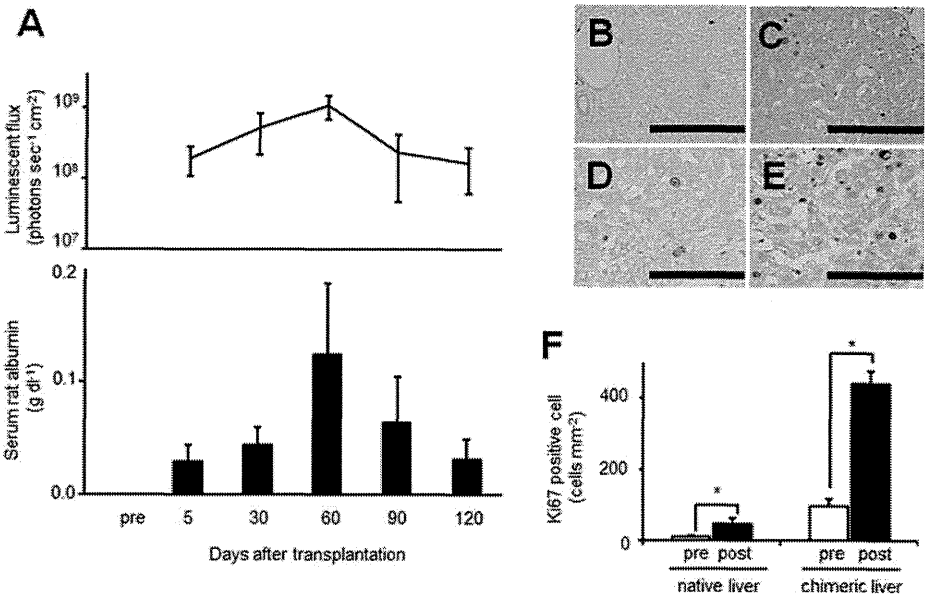

FIGURE 4. A, Luminescence (line) and albumin production (column) from transplanted CLs in Nagase analbuminemia rat recipients ($n = 3$). Values are shown as the mean ± SEM; pre, pre-chimeric liver transplantation. B–F, Immunohistochemical analyses with Ki67. B, C, Recipient native and transplanted CLs, respectively, before host hepatectomy. D, E, Recipient remnant and CLs, respectively, 2 days after recipient left lobectomy. F, Numbers of Ki67-positive cells. Values are shown as the mean ± SEM; pre, prelobectomy; post, postlobectomy.

Self-Regenerative Capacity of Transplanted CL

Ki67 immunohistochemical analyses revealed that Ki67-positive cells were significantly increased in the CLs and in the remnant native livers at 2 days after the left lobectomy in the recipients, as compared with those sampled before the hepatectomy (Fig. 4B–F), suggesting the proliferative potential of the transplanted CLs.

DISCUSSION

The chronic shortage of liver grafts has led to extended criteria for grafts from both deceased[19,20] and living donors,[21] along with ethical issues related to organ trafficking and transplant tourism.[22] Although alternative therapies, such as hepatocyte transplantation,[23] transplantation from non–heart beating donors,[24] bioartificial liver,[25] and xenotransplantation,[26,27] have been intensively investigated to address this situation, none has been found practical because of low stability, low availability, and high antigenicity.

Regenerative approaches have recently been applied to develop engineered organs by focusing on native organs as scaffolds. An approach using a decellularized organ matrix enabled regeneration of syngeneic cells in an animal model,[5,6] though cell repopulation efficiency was still low in ex vivo conditions. Another study injected blastocysts with xenogeneic pluripotent stem cells to produce a chimeric pancreas in a rodent model.[7] However, ubiquitous chimerism in scaffold animals has led to ethical concerns about the formation of chimeric brains and genitalia. Thus, effective and organ-specific engineering is required.

We have developed a strategy to create engineered chimeric "organ" livers with autologous or allogeneic human hepatocytes and other nonparenchymal components from xenogeneic scaffolds in transgenic pigs. This method enables utilization of patent hepatocytes and allogeneic donor cells, and the organogenetic potential in living animals contributes to rapid and timely production of CLs. Moreover, pretreatment with drugs or gene induction in the donor animal may be useful before transplantation.

In this study, we successfully created a rodent model to generate organ-specific engineered CLs, followed by their transplantation. CLs were created in uPA/SCID mice, whose native hepatocytes are injured through accumulation of urokinase-type plasminogen and provide a favorable niche for effective repopulation of transplanted hepatocytes from rats[28] and humans,[11] with a replacement rate greater than 90%.[12] Using hepatocytes derived from transgenic rats with

luciferase or LacZ genes, we found that transplanted hepatocytes in mice spread promptly and stably maintained their viability. Rat albumin production and histological analyses also indicated stable functions and structures of the CLs. These results demonstrated the advantages of CLs with effective productivity and maintenance. Because the CLs were one-eighth smaller than the rat native livers, we transplanted in an auxiliary manner without a hepatectomy or removal of the recipient liver. In addition, we removed the recipient's left kidney to utilize the left renal artery and vein as afferent and efferent vessels, respectively. We considered that a left nephrectomy would not have a large impact on our aim to investigate chimeric liver transplantation feasibility, whereas it might have an influence on recipient's survival. Moreover, though clinical liver transplantation and most rat liver transplantation models reconstruct portal vein circulation, we left it unanastomosed, as we previously reported in a rat auxiliary liver transplantation model,[17] in which the transplanted livers maintained their histological structure.

This analysis revealed severe rejection toward xenogeneic components, resulting in disappearance of luminescence in CLs without immunosuppression. Because humoral rejection was suspected in xenorejection toward the vascular endothelium,[29] we used cyclophosphamide to suppress antibody production in addition to tacrolimus.[18] Our results showed improvement in graft survival in the immunosuppressed groups. TAC(+)CPA(+) showed higher luminescence as compared with TAC(+)CPA(−), though there was no statistical difference between them. On the other hand, histological results showed the superiority of TAC(+)CPA(+). We speculated that these findings indicated antibody-mediated rejection even in Chimeric liver transplantation and that appropriate combination therapies might improve graft survival. Although we previously hypothesized that syngeneic parenchyma might function to protect against rejection toward xenocomponents,[30] the reaction to mouse-origin tissues remained without obvious evidence of attenuation. Further studies to investigate the effects of hepatocytes and specific targets of rejection are required, including those that focus on other aspects such as genetic expressions.[31]

In clinical liver transplantation, thrombotic events can result in graft failure.[32] Ultrasonography showed arterial and venous flow in transplanted CLs even after 6 months, which indicated patency of the anastomosed vessels. We also investigated rat albumin in Nagase analbuminemia rat recipients and demonstrated stable production for a long period. Although the liver possesses a variety of functions and markers,[3,6] albumin analysis showed functions specific to transplanted CLs in Nagase analbuminemia rats with intact livers, which functioned normally except for albumin production. We regarded this result to be preferable in regard to our aim to investigate the feasibility of Chimeric liver transplantation to show those functions in vivo. Interestingly, we found stable luminescence in transplanted CLs of Nagase analbuminemia rat recipients whose hepatocytes were allogeneic to those of other recipients ($RT1^l$ vs $RT1^a$), suggesting the possibility of a hepatocyte bank for use in producing CLs in clinical settings.

Ki67 analyses showed that hepatocytes in the transplanted CLs maintained proliferation potential. Patients with end-stage liver disease are thought to manifest increasing serum hepatotropic growth signals, such as hepatocyte growth factor.[33] It is expected that CLs will have the potential to respond to such signals to maintain and improve viability after transplantation.

Judging from recent technological achievements in transgenic animals, and ethical issues related to primate usage and practical issues of availability and body size, transgenic pigs represent a major candidate for scaffold animals. Although transgenic pigs such as alpha-1,3-galactosyltransferase gene knockout and human decay accelerating factor transgenic pigs show reduced immunological responses toward the host, complete rejection suppression remains difficult and development of appropriate immunosuppressive protocols is important. Moreover, replacement of nonhepatocyte components, especially vascular endothelium, in the CLs of scaffold pigs or development of humanized pigs is expected. However, utilization of xenogeneic porcine scaffolds raise concerns about xenozoonosis such as porcine endogenous retrovirus,[34,35] though the practical possibility of transmission remains uncertain and some reports have shown results without obvious infection.[36] Nevertheless, cautious and longer investigations are indispensable to secure patient safety.

Although further studies that compare conventional liver transplantation models with this model and larger animal models are needed, the realization of this bioengineering strategy with cell sources and transgenic animals might ultimately lead to replacement of human grafts and achievement of liver transplantation without human donors. These results should provide an important contribution toward scaffold-focused engineering of livers and engineered organ transplantation.

CONCLUSIONS

Engineered CLs were successfully transplanted and showed maintenance of function and structure for a long period. Our results suggest that such CLs have potential to be utilized as alternative grafts.

ACKNOWLEDGMENTS

The authors thank J. K. Critser (University of Missouri) for the insightful discussion and S. Enosawa (National Center for Child Health and Development) for the technical expertise regarding hepatocyte isolation. Transgenic rat embryos are available from the National Bio Resource Project for the Rat (nbrprat@anim.med.kyoto-u.ac.jp), and the Rat Resource & Research Center (Dr. Elizabeth Bryda.; RRRC, http://www.rrrc.us/) in USA.

REFERENCES

1. Thuluvath PJ, Guidinger MK, Fung JJ, et al. Liver transplantation in the United States, 1999–2008. *Am J Transplant.* 2010;10:1003–1019.
2. Yeh H, Smoot E, Schoenfeld DA, et al. Geographic inequity in access to livers for transplantation. *Transplantation.* 2011;91:479–486.
3. Ohashi K, Yokoyama T, Yamato M, et al. Engineering functional two- and three-dimensional liver systems in vivo using hepatic tissue sheets. *Nat Med.* 2007;13;880–885.
4. Soto-Gutiérrez A, Kobayashi N, Rivas-Carrillo JD, et al. Reversal of mouse hepatic failure using an implanted liver-assist device containing ES cell-derived hepatocytes. *Nat Biotechnol.* 2006;24:1412–1419.
5. Ott HC, Matthiesen TS, Goh SK, et al. Perfusion-decellularized matrix: using nature's platform to engineer a bioartificial heart. *Nat Med.* 2008;14:213–221.
6. Uygaun BE, Soto-Gutierrez A, Yagi H, et al. Organ reengineering through development of a transplantable recellularized liver graft using decellularized liver matrix. *Nat Med.* 2010;16:814–820.
7. Kobayashi T, Yamaguchi T, Hamanaka S, et al. Generation of rat pancreas in mouse by interspecific blastocyst injection of pluripotent stem cells. *Cell.* 2010;142:787–799.
8. Ekser B, Rigotti P, Gridelli B, et al. Xenotransplantation of solid organs in the pig-to-primate model. *Transpl Immunol.* 2009;21:87–92.
9. Klymiuk N, Aigner B, Brem G, et al. Genetic modification of pigs as organ donors for xenotransplantation. *Mol Reprod Dev.* 2010;77:209–221.
10. Locke JE, Sun Z, Warren DS, et al. Generation of humanized animal livers using embryoid body-derived stem cell transplant. *Ann Surg.* 2008;248;487–493.
11. Mercer DF, Schiller DE, Elliott JF, et al. Hepatitis C virus replication in mice with chimeric human livers. *Nat Med.* 2001;7:927–933.
12. Tateno C, Yoshizane Y, Saito N, et al. Near completely humanized liver in mice shows human-type metabolic responses to drugs. *Am J Pathol.* 2004;165:901–912.

13. Hakamata Y, Murakami T, Kobayashi E. "Firefly rats" as an organ/cellular source for long-term in vivo bioluminescent imaging. *Transplantation*. 2006;81:1179–1184.
14. Horie M, Sekiya I, Muneta T, et al. Intra-articular injected synovial stem cells differentiate into meniscal cells directly and promote meniscal regeneration without mobilization to distant organs in rat massive meniscal defect. *Stem Cells*. 2009;27:878–887.
15. Oren R, Dabeva MD, Petkov PM, et al. Restoration of serum albumin levels in Nagase analbuminemic rats by hepatocyte transplantation. *Hepatology*. 1999;29:75–81.
16. Enosawa S, Suzuki S, Li XK, et al. Higher efficiency of retrovirus transduction in the late stage of primary culture of hepatocytes from nontreated than from partially hepatectomized rat. *Cell Transplant*. 1998;7:413–416.
17. Rong Xiu D, Hishikawa S, Sato M, et al. Rat auxiliary liver transplantation without portal vein reconstruction: comparison with the portal vein-arterialized model. *Microsurgery*. 2001;21:189–195.
18. Murase N, Starzl TE, Demetris AJ, et al. Hamster-to-rat heart and liver xenotransplantation with FK506 plus antiproliferative drugs. *Transplantation*. 1993;55:701–708.
19. Durand F, Renz JF, Alkofer B, et al. Report of the Paris consensus meeting on expanded criteria donors in liver transplantation. *Liver Transpl*. 2008;14:1694–1707.
20. Renz JF, Kin C, Kinkhabwala M, et al. Utilization of extended donor criteria liver allografts maximizes donor use and patient access to liver transplantation. *Ann Surg*. 2005;242:556–565.
21. Trotter JF, Adam R, Lo CM, et al. Documented deaths of hepatic lobe donors for living donor liver transplantation. *Liver Transpl*. 2006;12:1485–1488.
22. Steering Committee of the Istanbul Summit. Organ trafficking and transplant tourism and commercialism: the Declaration of Istanbul. *Lancet*. 2008;372:5–6.
23. Dhawan A, Puppi J, Hughes RD, et al. Human hepatocyte transplantation: current experience and future challenges. *Nat Rev Gastroenterol Hepatol*. 2010;7:288–298.
24. Selck FW, Grossman EB, Ratner LE, et al. Utilization, outcomes, and retransplantation of liver allografts from donation after cardiac death: implications for further expansion of the deceased-donor pool. *Ann Surg*. 2008;248:599–607.
25. Demetriou AA, Brown RS, Busuttil RW, et al. Prospective, randomized, multicenter, controlled trial of a bioartificial liver in treating acute liver failure. *Ann Surg*. 2004;239:660–670.
26. Starzl TE, Fung J, Tzakis A, et al. Baboon-to-human liver transplantation. *Lancet*. 1993;341:65–71.
27. Ekser B, Gridelli B, Tector AJ, et al. Pig liver xenotransplantation as a bridge to allotransplantation: which patients might benefit? *Transplantation*. 2009;88:1041–1049.
28. Giannini C, Morosan S, Tralhao JG, et al. A highly efficient, stable, and rapid approach for ex vivo human liver gene therapy via a FLAP lentiviral vector. *Hepatology*. 2003;38:114–122.
29. Ghebremariam YT, Smith SA, Anderson JB, et al. Intervention strategies and agents mediating the prevention of xenorejection. *Ann N Y Acad Sci*. 2005;1056:123–143.
30. Goto S, Lord R, Kobayashi E, et al. Novel immunosuppressive proteins purified from the serum of liver-retransplanted rats. *Transplantation*. 1996;61:1147–1151.
31. Tahara K, Murakami T, Fujishiro J, et al. Regeneration of the rat neonatal intestine in transplantation. *Ann Surg*. 2005;242:124–132
32. Bekker J, Ploem S, de Jong KP. Early hepatic artery thrombosis after liver transplantation: a systematic review of the incidence, outcome and risk factors. *Am J Transplant*. 2009;9:746–757.
33. Tomiya T, Omata M, Imamura H, et al. Impaired liver regeneration in acute liver failure: the significance of cross-communication of growth associated factors in liver regeneration. *Hepatol Res*. 2008;38:S29–S33.
34. Mueller NJ, Takeuchi Y, Mattiuzzo G, at al. Microbial safety in xenotransplantation. *Curr Opin Organ Transplant*. 2011;16:201–206.
35. Onions D, Cooper DK, Alexander TJ, et al. An approach to the control of disease transmission in pig-to-human xenotransplantation. *Xenotransplantation*. 2000;7:143–155.
36. Michaels MG, Kaufman C, Volberding PA, et al. Baboon bone-marrow xenotransplant in a patient with advanced HIV disease: case report and 8-year follow-up. *Transplantation*. 2004;78:1582–1589.

Journal of the Neurological Sciences 324 (2013) 190–194

Contents lists available at SciVerse ScienceDirect

Journal of the Neurological Sciences

journal homepage: www.elsevier.com/locate/jns

Short communication

Failure of mefloquine therapy in progressive multifocal leukoencephalopathy: Report of two Japanese patients without human immunodeficiency virus infection

Zen Kobayashi [a,*,1], Miho Akaza [a,1], Yoshiyuki Numasawa [a], Shoichiro Ishihara [b], Hiroyuki Tomimitsu [a], Kazuo Nakamichi [c], Masayuki Saijo [c], Tomohiro Morio [d], Norio Shimizu [e], Nobuo Sanjo [b], Shuzo Shintani [a], Hidehiro Mizusawa [b]

[a] Department of Neurology, JA Toride Medical Center, Ibaraki, Japan
[b] Department of Neurology and Neurological Science, Tokyo Medical and Dental University, Tokyo, Japan
[c] Department of Virology I, National Institute of Infectious Diseases, Tokyo, Japan
[d] Department of Pediatrics and Developmental Biology, Tokyo Medical and Dental University, Tokyo, Japan
[e] Department of Virology, Division of Virology and Immunology, Medical Research Institute, Tokyo Medical and Dental University, Tokyo, Japan

ARTICLE INFO

Article history:
Received 24 August 2012
Received in revised form 3 November 2012
Accepted 6 November 2012
Available online 22 November 2012

Keywords:
Mefloquine
JC virus
Progressive multifocal leukoencephalopathy
Human immunodeficiency virus
Blood–brain barrier
CD4

ABSTRACT

Although progressive multifocal leukoencephalopathy (PML) cases showing responses to mefloquine therapy have been reported, the efficacy of mefloquine for PML remains unclear. We report on the failure of mefloquine therapy in two Japanese patients with PML unrelated to human immunodeficiency virus. One of the patients was a 47-year-old male who had been treated with chemotherapy for Waldenström macroglobulinemia, and the other was an 81-year-old male with idiopathic $CD4^+$ lymphocytopenia. Diagnosis of PML was established based on MRI findings and increased JC virus DNA in the cerebrospinal fluid in both patients. Mefloquine was initiated about 5 months and 2 months after the onset of PML, respectively. During mefloquine therapy, clinical and radiological progression was observed, and JC virus DNA in the cerebrospinal fluid was increased in both patients. Both patients died about 4 months and 2 months after initiation of mefloquine, respectively. Further studies are necessary to clarify the differences between mefloquine responders and non-responders in PML.

1. Introduction

Progressive multifocal leukoencephalopathy (PML) is a brain disorder caused by JC polyomavirus, which causes death in one-half of patients within 1 year [1]. Primary infection usually occurs during childhood and is often asymptomatic. The initial site of JC virus (JCV) infection is thought to be the tonsils, and it is then carried by lymphocytes to the kidneys and bone marrow. Reactivation of JCV occurs due to severe cellular immunodeficiency, and the virus crosses the blood–brain barrier (BBB) and infects oligodendrocytes, causing widespread demyelinating lesions. A recent study revealed promyelocytic leukemia nuclear bodies as an intranuclear target of JCV [2].

A study of 9675 cases of PML between 1998 and 2005 showed that 82% of patients had human immunodeficiency virus (HIV), 8.4% hematologic malignancies, 2.83% solid organ cancers, and 0.44% rheumatologic diseases [3]. Recently, a new category of PML patients has emerged among patients treated with immunomodulatory medications including natalizumab, rituximab, and efalizumab. PML may also occur in patients with minimal or occult immunosuppression including idiopathic $CD4^+$ lymphocytopenia [4]. In Japan, the proportion of hematological malignancies or rheumatologic diseases as underlying diseases is relatively high, whereas that of HIV infection is low [5,6].

The estimated probability of survival at 1 year is reported to be 52% in HIV related PML [1] and variable in PML unrelated to HIV among reports. Some patients with PML do survive for extended periods of time after diagnosis [7,8]. Survival in PML is influenced by the presence of JCV-specific cytotoxic T-lymphocytes, $CD4^+$ cell counts, or JCV DNA levels [1,9]. One study reported that estimated 1-year survival was 48% in patients with HIV related PML with $CD4^+$ cell counts $<200/\mu l$ at PML diagnosis compared to 67% in those with $CD4^+$ cell counts $>200/\mu l$ [1]. Another study showed that JCV DNA levels >4365 copies/ml of cerebrospinal fluid (CSF) correlated significantly with shorter survival in patients with HIV related PML not receiving highly active antiretroviral therapy (HAART) [9].

To date, although antiviral drugs such as cytarabine and cidofovir show activity against JCV *in vitro* [10,11], large clinical studies have failed to establish the efficacies of these drugs in the treatment of PML [12–14]. The reason for this may be that these drugs are not able to cross the BBB and accumulate throughout the entire brain parenchyma at a dose sufficient to suppress JCV proliferation [15].

* Corresponding author at: Department of Neurology, JA Toride Medical Center, 2-1-1 Hongo, Toride, Ibaraki 302-0022, Japan.
E-mail address: zen@bg7.so-net.ne.jp (Z. Kobayashi).
[1] The first two authors equally contributed to this work.

0022-510X/$ – see front matter
http://dx.doi.org/10.1016/j.jns.2012.11.004

In 2008, mefloquine, an anti-malarial drug, was reported to show activity against JCV *in vitro* [15]. Since then, there have been at least 5 reported cases of PML in which mefloquine was effective [16–20]. In contrast, a recent mefloquine trial of 24 patients with PML (21 HIV-positive and 3 HIV-negative) reported failure in reducing JCV DNA levels in the CSF [21], although it is pending publication. Because there have been no reports describing the details of PML patients demonstrating mefloquine treatment failure, we report two HIV-negative patients with PML in whom mefloquine was not effective.

2. Case reports

2.1. Case 1

A 47-year-old male presented with progressive left hemiparesis. The patient had been treated with chemotherapy including rituximab for Waldenström macroglobulinemia for six years in our hospital. The interval between the last administration of rituximab and occurrence of hemiparesis was about 1 month. Diffusion weighted images (DWI) of brain MRI about 3 months after the onset of hemiparesis demonstrated high intensity areas with internal low intensity areas in the white matter of the right frontal lobe. The apparent diffusion coefficient (ADC) values of the lesion were increased. Because serum IgM had been prominently elevated (around 5000 mg/dl) in association with Waldenström macroglobulinemia, we presumed that the hyperviscosity syndrome resulted in brain infarction.

About 4 months after the onset of hemiparesis, the patient was admitted to our hospital because a convulsion occurred in the left upper and lower limbs. At that time, the patient did not receive any immunosuppressive therapy. On admission, neurological examination revealed upper limb-dominant left hemiparesis, and Babinski's sign and Chaddock's reflex on the left. MRI on admission demonstrated lesion expansion and extension to the right parietal and insular white matter, right putamen, right internal capsule, right thalamus, corpus callosum, left frontal white matter, and midbrain. There was no edema or gadolinium-enhanced lesions. Peripheral blood tests showed white blood cell count (WBC): 3790/μl (normal range: 4500–9000), hemoglobin: 10.4 g/dl (normal range: 13–16), and platelet count: 3.7×10^4/μl (normal range $15–30\times10^4$), indicating pancytopenia. C-reactive protein (CRP) was below 0.1 mg/dl. Testing for HIV was negative. On the next day of admission, a nasogastric feeding tube was inserted because of dysphagia. Four days after admission, CSF examination demonstrated cell count: 1 cell per 3 μl, total protein: 97 mg/dl, and glucose: 67 mg/dl. PCR was positive for JCV DNA in the CSF and detected 1200 copies/ml of DNA. A diagnosis of PML was established based on MRI findings and increased JCV DNA in the CSF.

After diagnosis, the patient developed right hemiparesis and apraxia of speech. Brain MRI 18 days after admission demonstrated lesion expansion and extension to the left insular white matter and left putamen (Fig. 1A). The JCV DNA copy number in the CSF was increased to 4300 copies/ml. $CD4^+$ cell count of the peripheral blood was 219/μl (normal range: 500–1300). Nineteen days after admission, about 5 months after the onset of PML, mefloquine was initiated at a dose of 275 mg/day orally for 3 days, followed by 275 mg once a week [17]. We used Mephaquin Hisamitsu tablets (Hisamitsu Pharmaceutical, Tosu, Japan), which show maximum concentration (C_{max}) of 3.1 μM, time at which C_{max} is observed (T_{max}) of 5.2 h, and terminal half-life (T1/2) of 400.1 h when 1100 mg of drug is once administered. Treatment with mefloquine was approved by the Ethics Committee in our hospital. We obtained written, informed consent from the patient's family. We also used 1 mg/day of risperidone, a 5HT2A receptor blocker at the same time. After initiation of mefloquine, we observed no symptoms suggestive of mefloquine neurotoxicity such as nausea, dizziness, sleep disturbances, anxiety, and psychosis [22]. Eight days after initiation of mefloquine, the JCV DNA copy number in the CSF was increased to 150,000 copies/ml, and the dose of mefloquine was returned to 275 mg/day for 3 days per week (Fig. 2).

However, the JCV DNA copy number in the CSF 22 days after initiation of mefloquine was increased to 850,000 copies/ml. Because of severe aspiration pneumonia, tracheotomy was performed 37 days after initiation of mefloquine. Brain MRI 38 days after initiation of mefloquine demonstrated lesion expansion and extension to the right temporal and occipital white matter and pons (Fig. 1B). The JCV DNA copy number in the CSF 50 days after initiation of mefloquine increased to 3,700,000 copies/ml. Changes in the JCV DNA load are shown in Fig. 2. Brain MRI about 3 months after initiation of mefloquine demonstrated lesion expansion and extension to the left temporal and parietal white matter, left internal capsule, left thalamus, and medulla oblongata (Fig. 1C). The patient died of respiratory failure about 4 months after initiation of mefloquine. The total clinical course of PML was about 9 months. Autopsy could not be performed.

2.2. Case 2

An 81-year-old male with a three-week history of gait disturbance presented with muscle cramp in the bilateral upper limbs and was taken to another hospital by ambulance. Past medical history included hypertension, hyperuricemia, chronic heart failure, and chronic renal failure due to renal sclerosis. A diagnosis of brain infarction of the

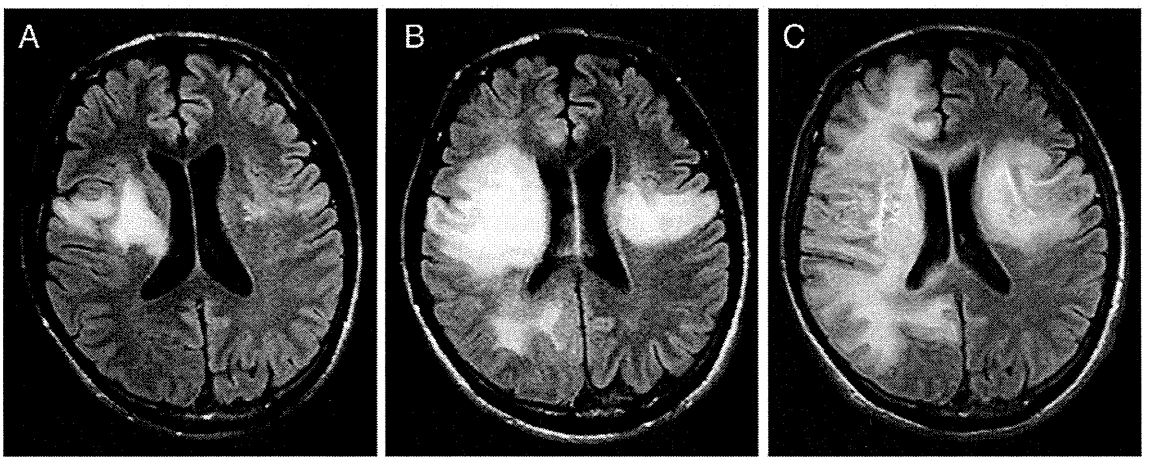

Fig. 1. A. Fluid-attenuated inversion recovery (FLAIR) sequence of brain MRI before initiation of mefloquine demonstrated high intensity areas in the white matter of the bilateral frontal lobes. B, C. FLAIR sequence of brain MRI 38 days (B) and about 3 months (C) after the initiation of mefloquine showed lesion expansion.

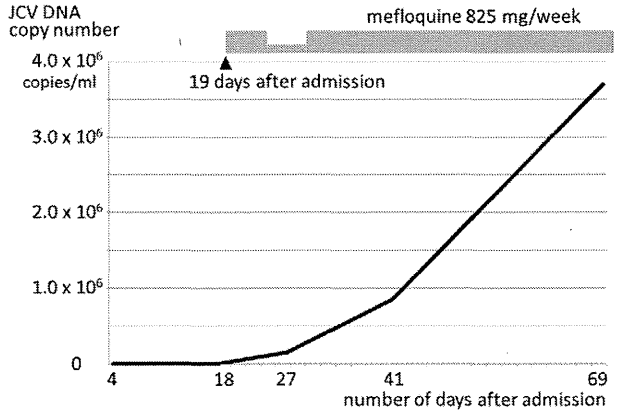

Fig. 2. Changes in the JCV DNA load of case 1 are shown. The JCV DNA copy number in the CSF was increased even after initiation of mefloquine.

subacute phase and the worsening of renal failure was made in the emergency room and the patient was transferred to our hospital.

Physical examination on admission demonstrated muscle cramp in the bilateral upper limbs and face, and right hemiparesis. Consciousness was slightly disturbed, but the orientation to time and place was preserved. Peripheral blood tests showed WBC: 5240/μl, hemoglobin: 7.8 g/dl, platelet count: 17.6×10^4/μl, albumin: 2.7 g/dl (normal range: 3.9–4.9), blood urea nitrogen (BUN): 147 mg/dl (normal range: 8–20), creatinine: 7.83 mg/dl (normal range: 0.6–1.1), creatinine kinase (CK): 445 IU/l (normal range 50–200), CRP: 0.3 mg/dl (normal range <0.1), and glucose: 103 mg/dl. Testing for HIV was negative. Hemodialysis was started on the next day of admission.

DWI of brain MRI 3 days after admission demonstrated high intensity areas in the white matter of the left frontal and parietal lobes and right parietal lobe. ADC values of the lesions were increased. Right hemiparesis progressed after admission, and 18 days after admission, the left hemiparesis emerged. Because of dysphagia, a nasogastric feeding tube was inserted 19 days after admission. CSF examination 20 days after admission demonstrated cell count: 6 cells per 3 μl, total protein: 35 mg/dl, and glucose: 60 mg/dl. PCR was positive for JCV DNA in the CSF, and detected 2223 copies/ml of DNA. A diagnosis of PML was established based on MRI findings and increased JCV DNA in the CSF.

Brain MRI 32 days after admission demonstrated lesion expansion and extension to the corpus callosum and right frontal white matter. Thirty six days after admission, the patient manifested akinetic mutism. Thirty eight days after admission, about 2 months after the onset of PML, mefloquine was initiated at a dose of 275 mg/day orally for 3 days per week. Treatment with mefloquine was approved by the Ethics Committee in our hospital. We obtained written, informed consent from the patient's family. At that time, the JCV DNA copy number in the CSF was increased to 2,790,000 copies/ml. The $CD4^+$ cell count of the peripheral blood was 294/μl. Because whole body CT demonstrated no mass lesions or abnormal lymph node swelling, underlying diseases causing immunodeficiency remained unclear in this patient.

After initiation of mefloquine, we observed no acute neurological deterioration suggesting mefloquine neurotoxicity. Brain MRI 15 days after initiation of mefloquine demonstrated lesion expansion and extension to the bilateral temporal and occipital white matter (Fig. 3A). Twenty nine days after initiation of mefloquine, the JCV DNA copy number in the CSF was increased to 24,075,000 copies/ml. Changes in the JCV DNA load are shown in Fig. 4. Brain MRI 31 days after initiation of mefloquine demonstrated lesion expansion (Fig. 3B). Thirty three days after initiation of mefloquine, hemodialysis was discontinued because of hypotension. The patient died 19 days later. The total clinical course of PML was about 4 months. Autopsy could not be performed.

3. Discussion

Because there is no known specific antiviral agent against JCV, we treated PML in the two HIV-negative patients with mefloquine based on case reports describing the efficacy of mefloquine for PML [16–20]. However, during mefloquine therapy, clinical and radiological progression was observed, and JCV DNA in the CSF was increased in both patients.

Our case 1 had been treated with chemotherapy including rituximab for Waldenström macroglobulinemia. The interval between the last administration of rituximab and diagnosis of PML was about 6 months. Although it is difficult to exclude the possibility that the immunodeficiency due to Waldenström macroglobulinemia itself was related to the occurrence of PML [23], rituximab is well known to cause PML [7]. Rituximab is an anti-CD20 monoclonal antibody that targets human B cells. The pathogenesis of rituximab in PML is considered to decrease B cells in the cerebral perivascular spaces, resulting in decreased antigen presentation to T cells and subsequent alterations in the cellular immune response [7]. One study reported that a median $CD4^+$ cell count was 216/μl in 25 patients who received rituximab [24]. The interval between the last administration of rituximab and

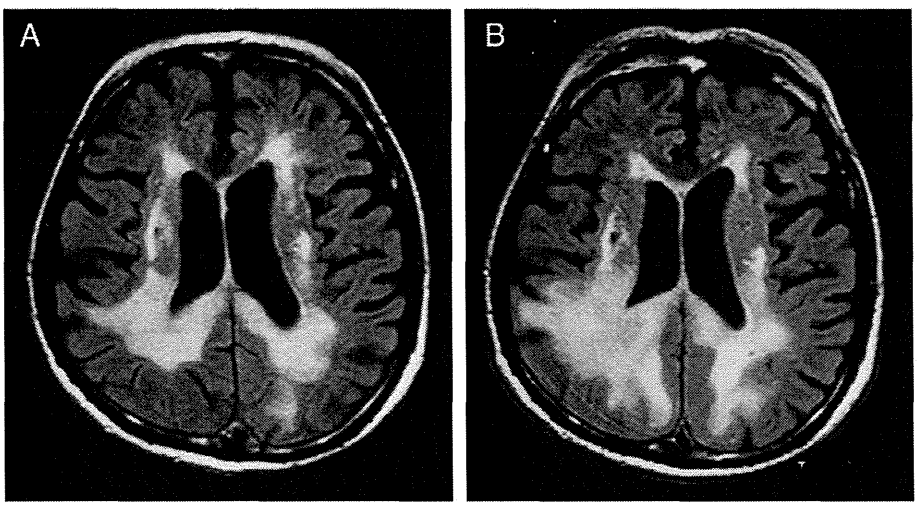

Fig. 3. A. FLAIR sequence of brain MRI 15 days after initiation of mefloquine demonstrated abnormal high intensity areas in the bilateral temporal and occipital white matter. B. FLAIR sequence of brain MRI 31 days after the initiation of mefloquine showed lesion expansion.

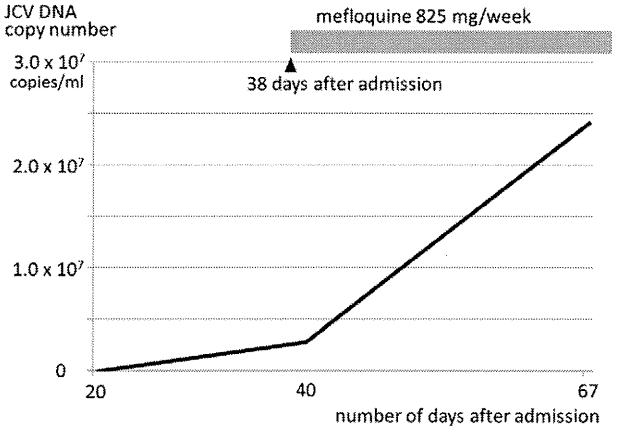

Fig. 4. Changes in the JCV DNA load of case 2 are shown. The JCV DNA copy number in the CSF was increased even after initiation of mefloquine.

diagnosis of PML has been reported to be 5.5 months [25]. Considering that 90% of patients with PML after rituximab therapy die [25], the unfavorable clinical course of our case 1 may be associated with the use of rituximab. In case 2, while $CD4^+$ lymphocytopenia was documented, there were no underlying diseases causing immunodeficiency. However, as PML may occur in patients with minimal or occult immunosuppression [4], idiopathic $CD4^+$ lymphocytopenia may be associated with the occurrence of PML in this patient.

Mefloquine is an anti-malarial drug used both for prophylaxis and treatment of chloroquine resistant *Plasmodium falciparum*. Because mefloquine is highly lipophilic and has a long terminal half-life of more than 1 week [26], a single dose of 15–25 mg/kg is used for treatment and 250 mg/week for prophylaxis. Among subjects administered 250 mg weekly, blood concentrations vary between 1 μM to 5 μM [27]. Mefloquine readily crosses the BBB, where active efflux by the P-glycoprotein membrane transporter prevents its accumulation in the brain [27].

In 2008, mefloquine was reported to show activity against JCV *in vitro* [15]. Brickelmaier et al. showed that mefloquine inhibits viral DNA replication, using quantitative PCR to quantify the number of viral copies in cultured cells. In this study, mefloquine reduced the number of infected cells by 50% or more at a concentration of 3.9 μM [15]. Brickelmaier et al. presumed that efficacious concentrations of mefloquine for PML are achieved in the brains of patients receiving approved doses of the drug [15].

Since the publication by Brickelmaier et al. [15], there have been at least 5 reported cases of PML in which mefloquine was effective [16–20]. The underlying diseases or conditions included sarcoidosis [16], umbilical cord blood transplant [17], HIV infection [18], and systemic lupus erythematosus [19]. $CD4^+$ cell counts in the peripheral blood of patients were described in 3 reports, and were 187/μl [18], 419/μl [17], and 420/μl [16], respectively. JCV DNA loads in the CSF before mefloquine therapy were available in these reports, and were 33,700 copies/ml [16], 535,500 copies/ml [18], and 911,175 copies/ml [17], respectively. The intervals between symptom onset and initiation of mefloquine therapy were about 3 months [17,19], 5 months [18], and 6 months [16,20], respectively. In 4 reports [16–19], the authors stated that PCR for JCV in the CSF became negative after mefloquine therapy. At present, the patients' background or laboratory data common among these cases showing responses to mefloquine therapy is unclear.

In contrast to these cases, a recent mefloquine trial of 24 patients with PML (21 HIV-positive and 3 HIV-negative) reported failure in reducing JCV DNA levels in the CSF [21]. Participants took 250 mg of mefloquine 4 times daily, followed by 250 mg weekly. The failure of this trial and the poor outcome of our patients raise the possibility that the improvement observed in mefloquine therapy in reported PML patients [16–20] may actually reflect the natural favorable course of those patients.

At present, we cannot tell the difference in patient backgrounds or laboratory data between patients showing responses to mefloquine [16–20] and our patients. Regarding the presence of both mefloquine responders and non-responders in PML, Nevin stated that responses to mefloquine may correlate with polymorphisms in the *MDR1* gene coding for P-glycoprotein that affect drug efflux across the BBB [28]. In cases of unsuccessful treatment of PML, active efflux as a result of drug induced upregulation of P-glycoprotein expression in the BBB may be preventing therapeutic concentrations of mefloquine [28]. From this point of view, co-administration of P-glycoprotein inhibitors or substrates such as risperidone may be recommended in the treatment of PML [27]. On the other hand, considering the failure of the mefloquine trial and the poor outcome of our patients, re-evaluation of the anti-JCV activity of mefloquine may be required. If the anti-JCV activity of mefloquine is verified again, further studies are necessary to clarify whether the response to mefloquine in PML is influenced by the presence of HIV infection, $CD4^+$ cell counts, JCV DNA levels in the CSF, blood concentration of mefloquine, interval between disease onset and initiation of therapy, or *MDR1* polymorphism.

Conflict of interest statement

The authors have no conflicts of interest.

Acknowledgment

The authors thank Dr. Takayoshi Ito, Tamaki Kuyama, and Yuji Nakamura for clinical management of the patients. The study was financially supported by a grants-in-aid from the Research Committee of Prion Disease and Slow Virus Infection (H20-Nanchi-Ippan-013) and by those for Scientific Research from the Ministry of Education, Science, Sports and Culture of Japan (19790349 and 22790446), and by those for Research on HIV/AIDS (H24-AIDS-Wakate-002) from the Ministry of Health, Labour and Welfare of Japan.

References

[1] Marzocchetti A, Tompkins T, Clifford DB, Gandhi RT, Kesari S, Berger JR, et al. Determinants of survival in progressive multifocal leukoencephalopathy. Neurology 2009;73:1551-8.
[2] Shishido-Hara Y. Progressive multifocal leukoencephalopathy and promyelocytic leukemia nuclear bodies: a review of clinical, neuropathological, and virological aspects of JC virus-induced demyelinating disease. Acta Neuropathol 2010;120:403-17.
[3] Molloy ES, Calabrese LH. Progressive multifocal leukoencephalopathy: a national estimate of frequency in systemic lupus erythematosus and other rheumatic diseases. Arthritis Rheum 2009;60:3761-5.
[4] Gheuens S, Pierone G, Peeters P, Koralnik IJ. Progressive multifocal leukoencephalopathy in individuals with minimal or occult immunosuppression. J Neurol Neurosurg Psychiatry 2010;81:247-54.
[5] Kishida S. Progressive multifocal leukoencephalopathy—epidemiology, clinical pictures, diagnosis and therapy. Brain Nerve 2007;59:125-37.
[6] Mizusawa H, Kishida S, Saijo M, Yukishita M, Shishido-Hara Y, Sawa H, et al. Progressive multifocal leukoencephalopathy (PML). Rinsho Shinkeigaku 2011;51:1051-7.
[7] Tan CS, Koralnik IJ. Progressive multifocal leukoencephalopathy and other disorders caused by JC virus: clinical features and pathogenesis. Lancet Neurol 2010;9:425-37.
[8] Rueger MA, Miletic H, Dorries K, Wyen C, Eggers C, Deckert M, et al. Long-term remission in progressive multifocal leukoencephalopathy caused by idiopathic CD4+ T lymphocytopenia: a case report. Clin Infect Dis 2006;42:e53-6.
[9] Bossolasco S, Calori G, Moretti F, Boschini A, Bertelli D, Mena M, et al. Prognostic significance of JC virus DNA levels in cerebrospinal fluid of patients with HIV-associated progressive multifocal leukoencephalopathy. Clin Infect Dis 2005;40:738-44.
[10] Andrei G, Snoeck R, Vandeputte M, De Clercq E. Activities of various compounds against murine and primate polyomaviruses. Antimicrob Agents Chemother 1997;41:587-93.
[11] Hou J, Major EO. The efficacy of nucleoside analogs against JC virus multiplication in a persistently infected human fetal brain cell line. J Neurovirol 1998;4:451-6.
[12] Hall CD, Dafni U, Simpson D, Clifford D, Wetherill PE, Cohen B, et al. Failure of cytarabine in progressive multifocal leukoencephalopathy associated with human

immunodeficiency virus infection. AIDS Clinical Trials Group 243 Team. N Engl J Med 1998;338:1345-51.
[13] Marra CM, Rajicic N, Barker DE, Cohen BA, Clifford D, Donovan Post MJ, et al. A pilot study of cidofovir for progressive multifocal leukoencephalopathy in AIDS. AIDS 2002;16:1791-7.
[14] Wyen C, Hoffmann C, Schmeisser N, Wöhrmann A, Qurishi N, Rockstroh J, et al. Progressive multifocal leukencephalopathy in patients on highly active antiretroviral therapy: survival and risk factors of death. J Acquir Immune Defic Syndr 2004;37: 1263-8.
[15] Brickelmaier M, Lugovskoy A, Kartikeyan R, Reviriego-Mendoza MM, Allaire N, Simon K, et al. Identification and characterization of mefloquine efficacy against JC virus *in vitro*. Antimicrob Agents Chemother 2009;53:1840-9.
[16] Gofton TE, Al-Khotani A, O'Farrell B, Ang LC, McLachlan RS. Mefloquine in the treatment of progressive multifocal leukoencephalopathy. J Neurol Neurosurg Psychiatry 2011;82:452-5.
[17] Kishida S, Tanaka K. Mefloquine treatment in a patient suffering from progressive multifocal leukoencephalopathy after umbilical cord blood transplant. Intern Med 2010;49:2509-13.
[18] Naito K, Ueno H, Sekine M, Kanemitsu M, Ohshita T, Nakamura T, et al. Akinetic mutism caused by HIV-associated progressive multifocal leukoencephalopathy was successfully treated with mefloquine: a serial multimodal MRI study. Intern Med 2012;51:205-9.
[19] Beppu M, Kawamoto M, Nukuzuma S, Kohara N. Mefloquine improved progressive multifocal leukoencephalopathy in a patient with systemic lupus erythematosus. Intern Med 2012;51:1245-7.
[20] Hirayama M, Nosaki Y, Matsui K, Terao S, Kuwayama M, Tateyama H, et al. Efficacy of mefloquine to progressive multifocal leukoencephalopathy initially presented with parkinsonism. Clin Neurol Neurosurg 2012;114:728-31.
[21] Friedman R. News from the AAN Annual Meeting: malaria drug fails to fulfill promise in PML. Neurol Today 2011;11:8.
[22] Toovey S. Mefloquine neurotoxicity: a literature review. Travel Med Infect Dis 2009;7:2-6.
[23] Chiarchiaro J, McLendon RE, Buckley PJ, Laskowitz DT. Progressive multifocal leukoencephalopathy with occult Waldenström macroglobulinemia. J Clin Oncol 2010;28:e759-61.
[24] Laszlo D, Bassi S, Andreola G, Agazzi A, Antoniotti P, Balzano R, et al. Peripheral T-lymphocyte subsets in patients treated with rituximab–chlorambucil combination therapy for indolent NHL. Ann Hematol 2006;85:813-4.
[25] Carson KR, Evens AM, Richey EA, Habermann TM, Focosi D, Seymour JF, et al. Progressive multifocal leukoencephalopathy after rituximab therapy in HIV-negative patients: a report of 57 cases from the Research on Adverse Drug Events and Reports project. Blood 2009;113:4834-40.
[26] Looareesuwan S, White NJ, Warrell DA, Forgo I, Dubach UG, Ranalder UB, et al. Studies of mefloquine bioavailability and kinetics using a stable isotope technique: a comparison of Thai patients with falciparum malaria and healthy Caucasian volunteers. Br J Clin Pharmacol 1987;24:37-42.
[27] Nevin RL. Pharmacokinetic considerations in the repositioning of mefloquine for treatment of progressive multifocal leukoencephalopathy. Clin Neurol Neurosurg 2012;114:1204-5.
[28] Nevin RL. Neuropharmacokinetic heterogeneity of mefloquine in the treatment of progressive multifocal leukoencephalopathy. Intern Med 2012;51:2257.

blood

2013 121: 4512-4520
Prepublished online March 25, 2013;
doi:10.1182/blood-2012-08-450494

EZH2 overexpression in natural killer/T-cell lymphoma confers growth advantage independently of histone methyltransferase activity

Junli Yan, Siok-Bian Ng, Jim Liang-Seah Tay, Baohong Lin, Tze Loong Koh, Joy Tan, Viknesvaran Selvarajan, Shaw-Cheng Liu, Chonglei Bi, Shi Wang, Shoa-Nian Choo, Norio Shimizu, Gaofeng Huang, Qiang Yu and Wee-Joo Chng

Blood (print ISSN 0006-4971, online ISSN 1528-0020), is published weekly by the American Society of Hematology, 2021 L St, NW, Suite 900, Washington DC 20036.

Regular Article

LYMPHOID NEOPLASIA

EZH2 overexpression in natural killer/T-cell lymphoma confers growth advantage independently of histone methyltransferase activity

Junli Yan,[1] Siok-Bian Ng,[1-3] Jim Liang-Seah Tay,[3] Baohong Lin,[4] Tze Loong Koh,[4] Joy Tan,[3] Viknesvaran Selvarajan,[2,3] Shaw-Cheng Liu,[1] Chonglei Bi,[1] Shi Wang,[2] Shoa-Nian Choo,[2,3] Norio Shimizu,[5] Gaofeng Huang,[1] Qiang Yu,[6] and Wee-Joo Chng[1,3,4]

[1]Cancer Science Institute of Singapore, National University of Singapore, Singapore; [2]Department of Pathology, National University Health System, Singapore; [3]Yong Loo Lin School of Medicine, National University of Singapore, Singapore; [4]Department of Haematology-Oncology, National University Cancer Institute of Singapore, National University Health System, Singapore; [5]Department of Virology, Tokyo Medical and Dental University, Tokyo, Japan; and [6]Department of Cancer Biology and Pharmacology, Genome Institute of Singapore, Agency for Science, Technology and Research, Biopolis, Singapore

Key Points

- This study has uncovered an oncogenic role of EZH2 independent of its methyltransferase activity in NKTL.
- This study suggests that targeting EZH2 may have therapeutic usefulness in NKTL.

The role of enhancer of zeste homolog 2 (EZH2) in cancer is complex and may vary depending on the cellular context. We found that EZH2 is aberrantly overexpressed in the majority of natural killer/T-cell lymphoma (NKTL), an aggressive lymphoid malignancy with very poor prognosis. We show that EZH2 upregulation is mediated by MYC-induced repression of its regulatory micro RNAs and EZH2 exerts oncogenic properties in NKTL. Ectopic expression of EZH2 in both primary NK cells and NKTL cell lines leads to a significant growth advantage. Conversely, knock-down of EZH2 in NKTL cell lines results in cell growth inhibition. Intriguingly, ectopic EZH2 mutant deficient for histone methyltransferase activity is also able to confer growth advantage and rescue growth inhibition on endogenous EZH2 depletion in NKTL cells, indicating an oncogenic role of EZH2 independent of its gene-silencing activity. Mechanistically, we show that EZH2 directly promotes the transcription of cyclin D1 and this effect is independent of its enzymatic activity. Furthermore, depletion of EZH2 using a PRC2 inhibitor 3-deazaneplanocin A significantly inhibits growth of NK tumor cells. Therefore, our study uncovers an oncogenic role of EZH2 independent of its methyltransferase activity in NKTL and suggests that targeting EZH2 may have therapeutic usefulness in this lymphoma. (*Blood*. 2013;121(22):4512-4520)

Introduction

Nasal-type natural killer/T-cell lymphoma (NKTL) is an aggressive lymphoid malignancy associated with very poor survival outcomes.[1] A better understanding of the molecular abnormalities underlying this disease will provide important insights into the biology of this tumor; however, studies on NKTL are often limited by the lack of adequate tissue in small nasal biopsies and the presence of necrosis in biopsy specimens. Although more effective therapy is now available, treatment is still completely reliant on radiotherapy and combinations of chemotherapy.[2,3]

We and others have recently performed whole-genome gene expression studies and identify a number of genes that are differentially expressed in NKTL as well as pathways that are activated in NKTL. Enhancer of zeste homolog 2 (EZH2), one of the genes identified in our study to be aberrantly overexpressed in NKTL,[4] is a H3K27-specific histone methyltransferase and a component of the polycomb repressive complex 2 (PRC2), which plays a key role in the epigenetic maintenance of repressive chromatin mark. EZH2 protein contains a catalytic domain (SET domain) at the COOH-terminus that provides the methyltransferase activity. The catalytic domain must partner with other noncatalytic proteins, such as EED and SUZ12, to form the PRC2 in order to attain robust histone methyltransferase activity. Genome-wide approaches have demonstrated the importance of the PRC2 complex in the transcriptional regulation through H3K27 methylation and gene repression.[5]

Published literature reveals a number of possible mechanisms of EZH2 upregulation in different types of human cancers.[6] It has been shown that EZH2 expression can be transcriptionally activated by a fusion oncoprotein EWS-FLI1 in Ewing sarcoma.[7] EZH2 expression in the breast tumor–initiating cell population is particularly enhanced by hypoxia through HIF1a-mediated transactivation.[8] In addition to transcriptional regulation, the EZH2 transcript is known to be regulated by tumor suppressor micro RNAs (miRNAs). For example, miR-26a binds to and inhibits EZH2 transcript expression in B-cell lymphoma.[9] miR-101 is frequently lost in metastatic prostate cancer, thus releasing EZH2 from miR-101–mediated repression.[10] EZH2 can also be modulated by post-translational modifications through

Submitted August 16, 2012; accepted March 19, 2013. Prepublished online as *Blood* First Edition paper, March 25, 2013; DOI 10.1182/blood-2012-08-450494.

J.Y. and S.-B.N. contributed equally to this study.

The online version of this article contains a data supplement.

The publication costs of this article were defrayed in part by page charge payment. Therefore, and solely to indicate this fact, this article is hereby marked "advertisement" in accordance with 18 USC section 1734.

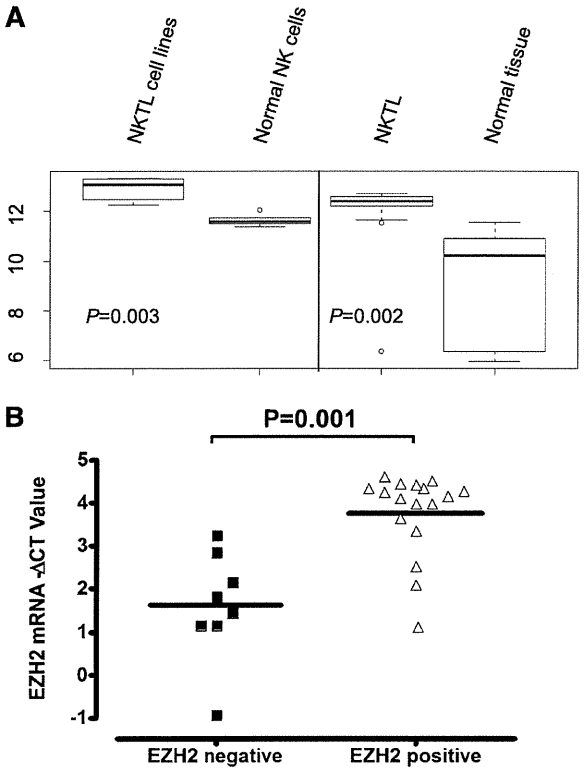

Figure 1. EZH2 mRNA levels are elevated in NKTL and cell lines. (A) Expression score for EZH2 mRNAs in NKTL GEP dataset. EZH2 gene expressions in NKTL FFPE samples were compared with that in respective normal FFPE tissue controls, as well as the NK cell lines and normal NK cells using significance analysis of microarray. (B) Correlation between EZH2 transcript levels determined by qRT-PCR and EZH2 protein levels measured by IHC for NKTL samples.

phosphorylation by AKT and cyclin-dependent kinase.[11,12] To the best of our knowledge, the mechanism of EZH2 overexpression in NKTL has not yet been described.

A high level of EZH2 expression is associated with aggressiveness and poor outcome in solid tumors such as prostate, breast, and endometrial cancers. The oncogenic role of EZH2 overexpression in these tumor types has been studied extensively. In human B-cell malignancies, mutations of Y641 and A677 have been documented to be associated with profoundly increased activity for methylated H3K27, which may promote the development of lymphoma.[13-15] On the other hand, recent discoveries of recurrent somatic *EZH2* mutations in myelodysplastic syndromes and myeloproliferative neoplasms indicate that inactivation of EZH2 may contribute to the pathogenesis of myeloid malignancies.[16,17] Genetic inactivation of EZH2 has also been identified in T-cell acute lymphoblastic leukemia, and the study by Ntziachristos and colleagues suggests a tumor suppressor role for EZH2 in human leukemia by a hitherto unrecognized dynamic interplay between oncogenic NOTCH1 and EZH2.[18] Taken together, the role of EZH2 and the underlying mechanisms of gene regulation by EZH2 in cancer are complex, and further studies need to be performed in a cell context–dependent manner.

In our study, we demonstrated the overexpression of EZH2 in NKTL, deciphered the molecular mechanisms underlying the overabundance of EZH2, and investigated its functional role as an oncogene in this disease. Contrary to our expectations, we found that EZH2 overexpression is not associated with H3K27 trimethylation in NKTL, and its oncogenic activity does not require its histone methyltransferase activity. Instead, EZH2 directly promotes cyclin D1 expression. Thus, this study demonstrates a noncanonic role of EZH2 in NKTL.

Methods

Immunohistochemistry

A total of 38 clinical cases of NKTL that fulfill the World Health Organization diagnostic criteria were used for immunohistochemistry (IHC) studies. The clinicopathologic data of the cases are included in supplemental Table 1. There were 27 cases that came from the tissue microarray used in our previous study (GEO accession no. GSE31377).[4] IHC analysis was performed for EZH2, Ki67, and H3K27me3 on 4-μm sections of NKTL using the conditions listed in supplemental Table 2. IHC study was also performed on cell blocks of normal NK cells for comparison. Appropriate positive tissue controls were used. Details of scoring and imaging are appended in the supplemental Methods.

Primary NK cell isolation and retroviral transduction

Highly purified (90%-99%) normal human NK cells were isolated and cultured as described previously.[19] Retroviruses were generated by transfection of empty plasmid vector polymorphonuclear neutrophil (pMN)-enhanced green fluorescence protein (EGFP) or vectors containing EZH2 using Fugene HD6 into Phoenix-amphotropic packaging cells. At 48 hours after transfection, the supernatants were collected and filtered. A total of 200 000 cells were mixed with 1.6 mL of retroviral supernatant in 12-well plates with 10 μg/mL of Polybrene added. The infection was repeated at 72 hours after transfection.

Luciferase reporter assay

The cyclin D1 (CCND1) promoter construct pGL4-CCND1-Luc has been described previously.[20] Cells were harvested 24 hours after transfection and were analyzed with the Dual Luciferase system (Promega). See the supplemental Methods and Materials for details.

ChIP assay

Chromatin immunoprecipitation (ChIP) assays were performed as described previously.[21] See the supplemental Methods and Materials for details of the antibodies used and primer sequences.

Western blotting

Cells were lysed in radioimmunoprecipitation assay buffer and were subjected to sonication. The primary antibodies used included cell-signaling antibody EZH2 (4905), H3K27me3 (07-449), H3K27me2 (9755), Total H3 (9715) and SantaCruz antibody CCND1 (DCS-6 and A12), and cleaved poly (ADP-ribose)polymerase (PARP; F2, sc-8007).

Full methods are provided in the supplemental information.

Results

EZH2 is overexpressed in NKTL

In our previously published genome-wide gene expression profiling (GEP) of extranodal nasal-type NKTL,[4] the EZH2 transcript level was significantly higher in NKTL compared with normal NK cells (Figure 1A). In corroboration with the GEP findings, we observed a significant percentage of cases (61%) showing positive expression of EZH2 protein in the tumor cells in our 38 cases of NKTL (tissue microarrays or whole-tissue sections) by IHC studies (supplemental Figure 1; supplemental Table 3), whereas the normal NK cells only showed a minimal level of EZH2 (staining in ≤5% cells). Indeed,

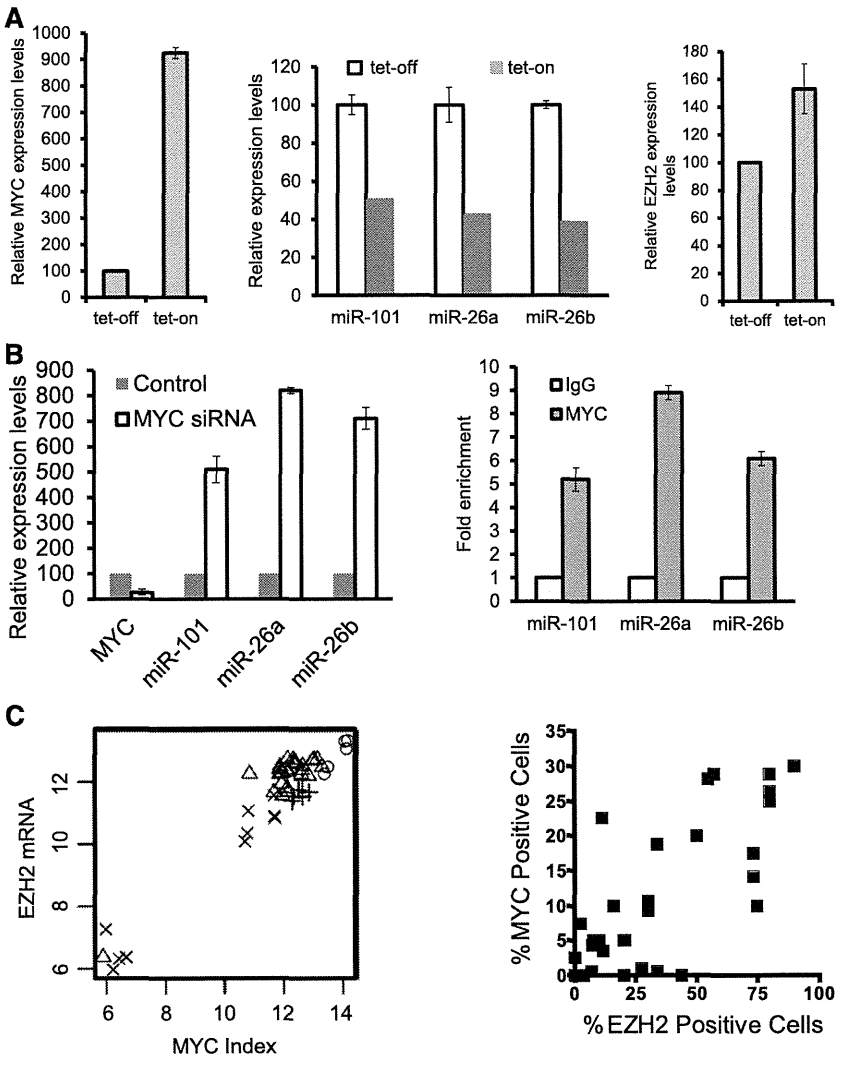

Figure 2. Inhibition of EZH2 expression by miRNA-101 and miRNA-26, which are suppressed by MYC in NKTL cells. (A, left) MYC induction by tet-on. MYC overexpression was induced by treating cells with doxycycline. MYC expression was quantified by qRT-PCR analysis. (A, middle) Decreased levels of miR-101, miR-26a, and miR-26b in NKYS upon MYC induction by tet-on. (A, right) MYC induction by tet-on increases EZH2 mRNA levels. (B, left) Depletion of MYC by siRNAs results in induction of miR-101, mir-26a, and miR-26b transcription in NKYS cells. Cells were transfected with MYC siRNA or nontargeting siRNA as a control. Cells were harvested 48 hours after transfection for mRNA analysis of miR-101 and miR-26 gene levels by real-time PCR. (B, right) ChIP-qPCR for endogenous MYC binding to miR-101, miR-26a, and miR-26b genes. Fold enrichment in the ChIP experiment represents the signal obtained after MYC immunoprecipitation followed by qPCR amplified by primer pairs that spanned gene promoters. (C, left) Correlation between MYC activation index and EZH2 mRNA levels. Cross: Normal tissue; Plus sign: Normal NK; Triangle: NKTL; Circle: Cell Lines. R>0.95, $P < 2.2*10^{-16}$. (C, right) Scatterplot showing the correlation between IHC MYC staining and EZH2 expression. Spearman correlation coefficient r for MYC v EZH2 = 0.76; $P < .0001$.

EZH2-positive samples have significantly higher EZH2 messenger RNA (mRNA) levels (Figure 1B). These data confirm that EZH2 is overexpressed in NKTL at both the mRNA and protein levels.

Loss of miR-26 and miR-101 contributes to the EZH2 upregulation in NKTL

Next, we sought to identify the mechanisms leading to EZH2 upregulation in NKTL. The genomic locus containing EZH2 is not commonly amplified in NKTL.[22] In our previous miRNA expression–profiling study, we found several miRNAs that were predicted to target EZH2 by various computational algorithms (supplemental Table 4) to be downregulated in NKTL.[19] Among these, the expression of miR-26a, miR-26b, and miR-101 has a significant inverse correlation with EZH2 when our previous GEP and miRNA profiling data were analyzed. miRNAs negatively regulate protein translation by predominantly destabilizing and, hence, decreasing their target mRNA levels.[23] In prostate, muscle, and B-cell lymphoma, miR-101, miR-26a, and miR-26b can negatively regulate EZH2 expression by binding to the highly conserved predicted binding sites within the 3′UTR of EZH2.[9,10] Using lentiviral transduction to express miR-101, miR-26a, and miR-26b in NKYS (supplemental Figure 2A, left), we observed that EZH2 expression was effectively attenuated (supplemental Figure 2A, right). These data suggest that EZH2 overexpression may be attributed to the deregulation of miR-101, miR-26a, and miR-26b in NK tumor cells.

MYC activation suppresses the expression of miR-26 and miR-101 in NKTL

As the genomic loci containing miR-101, miR-26a, and miR-26b are not recurrently deleted in the NKTL (data not shown), we looked for other mechanisms for their repression. On the basis of our previous study of gene expression in NKTL, which showed MYC activation,[4] and a recent paper showing that MYC activation can lead to repression of a many miRNAs in tumorigenesis,[24] we investigated whether MYC is involved in the suppression of miR-101 and miR-26 in malignant NK cells. When MYC expression was induced in NKYS cells using a tet-on system (Figure 2A, left), miR-101, miR-26a, and miR-26b was downregulated (Figure 2A, middle) with a corresponding (1.53-fold) increase in EZH2 mRNA (Figure 2A, right). Conversely, these 3 miRNAs were up-regulated by depletion of MYC using small interfering RNA (siRNA)–mediated knockdown (Figure 2B, left), and MYC depletion reduced EZH2 3′UTR luciferase reporter activity (supplemental

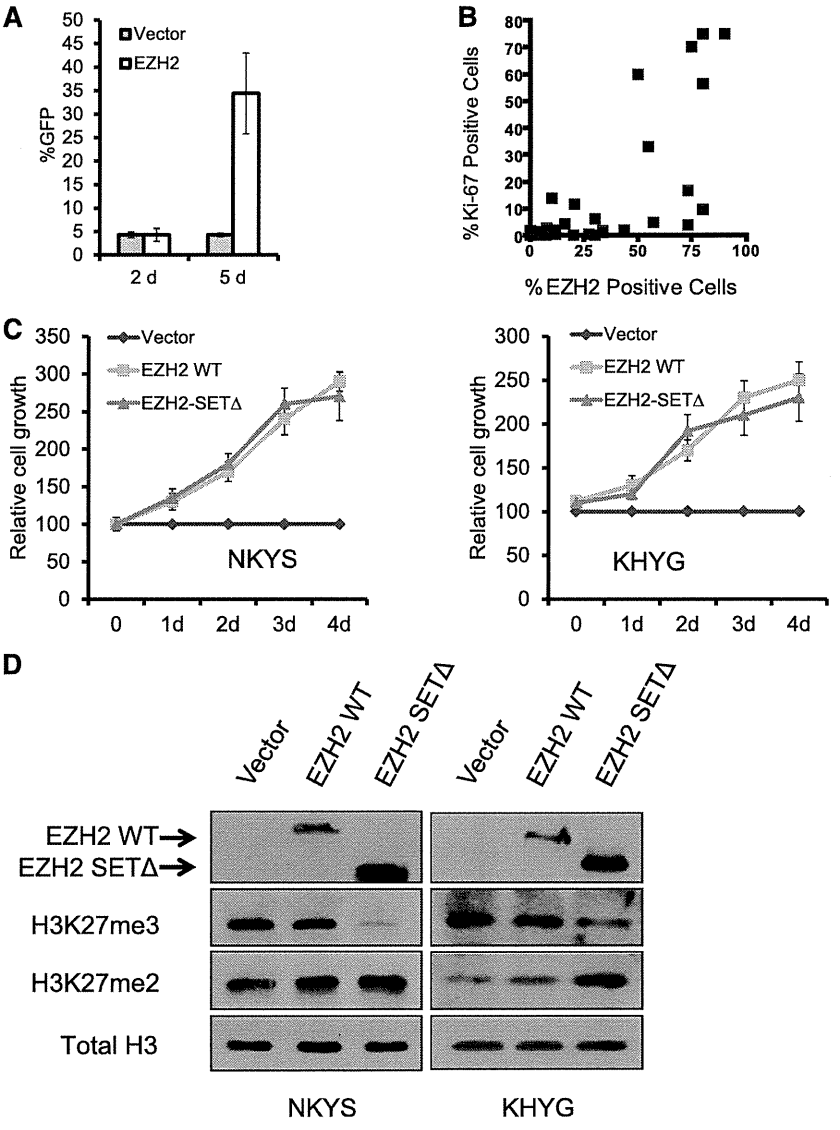

Figure 3. EZH2 overexpression in NKTL promotes cell growth independent of histone methyltransferase activity. (A) Primary NK cells transduced by EZH2 exhibit a growth advantage. Primary NK cells expressing ectopic EZH2 were monitored by a coexpressed GFP marker. Using our established viral infection protocol, we routinely obtained a transduction efficiency of 4.3% for normal NK cells. If EZH2 infection does not alter the cell growth, the EZH2-infected cell will not gain a growth advantage; thus, the percentage of GFP+ cells should remain at 4.3%. However, the percentage of GFP+ cells increased from approximately 4.3% at day 2 to ~34.4% at day 5, indicating an acquired growth advantage in these EZH2-infected cells. Antibiotic selection of positively infected cells was not done. (B) Scatterplot representation of the correlation between the percentage of Ki-67–positive cells and the percentage of EZH2-positive cells. Spearman correlation coefficient *r* for EZH2 v Ki67 = 0.73; $P < .0001$. (C) MTS proliferation assay showing that ectopic expression of EZH2 promotes cell growth of NKTL cell lines without requiring SET domain activity. Cells were cotransfected with pMAX-GFP and the control empty vector pcDNA4.1 or EZH2 expression plasmids. Cells transfected were subjected to proliferation assays for up to 96 hours. The cell growth (expressed as a percentage of the empty vector control) was determined by MTS assay as described in Materials and Methods. The mean values of triplicate samples are shown, and error bars indicate standard deviations. (D) Western blot analysis of EZH2, H3K27m3, and H3K27m2 in indicated samples. Expression of EZH2 WT and the SET-domain mutant was detected by the MYC-tag antibody. H3 was used as a loading control.

Figure 2B). However, this effect was still seen when the miR-101 and miR-26 binding sites in the EZH2 3′UTR were mutated, suggesting that other miRNAs or factors regulated by MYC may be involved. Furthermore, ChIP-quantitative polymerase chain reaction (qPCR) results revealed that MYC binds to the genomic locus of miR-26a and miR-26b (Figure 2B, right), consistent with previous reports.[24] Interestingly, it also revealed an association of MYC specifically with a conserved region upstream of miR-101 on chromosome 1 (Figure 2B, right). In summary, MYC activation suppresses the expression of miR-26a, miR-26b, and miR-101 in NKTL cell lines by direct binding to their genomic locus, and that MYC may stimulate EZH2 overexpression by repression of its negative regulatory miRNAs. Consistent with these in vitro findings, we observed a strong correlation between EZH2 transcript levels and MYC activation as measured by the gene expression–based MYC activation index[4] in our clinical GEP dataset (Figure 2C, left). In addition, there is also a positive correlation between the percentage of cells expressing EZH2 and nuclear MYC, which is a marker for MYC activation, detected by IHC analysis in NKTL tissue microarrays (Figure 2C, right). In addition, a significantly greater number of cells with nuclear MYC are detected in EZH2-positive samples (supplemental Figure 3A), suggesting that the data from NKTL cell lines are applicable to clinical samples.

EZH2 overexpression in NKTL confers a growth advantage independently of histone methyltransferase activity

Next, we investigated whether EZH2 is functionally important in NKTL. When EZH2 was introduced into primary NK cells purified from normal human peripheral blood, we observed an eightfold increase in the percentage of GFP(+) cells from day 2 to day 5 compared with vector control (Figure 3A), demonstrating that the overexpression of EZH2 is able to provide a growth advantage in normal primary human NK cells. We next analyzed the effect of increasing EZH2 on cell proliferation in NKTL cell lines. Ectopic expression of EZH2 through transient cotransfection with the GFP expression construct in NKYS cells for 3 days resulted in significantly higher percentage of viable GFP(+) cells in EZH2-transfected cells than in empty vector-transfected cells (supplemental Figure 4). This result suggests that EZH2 overexpression by transfection leads to

a competitive cell growth advantage. Consistent with these observations in the cell lines, a positive correlation between the expression of EZH2 and Ki-67, a marker of cell proliferation, was also observed in NKTL tumor samples (Figure 3B). Furthermore, EZH2 positivity is associated with a greater percentage of tumor cells expressing Ki-67 (supplemental Figure 3B).

Although EZH2 commonly exerts its oncogenic properties through H3K27 trimethylation (H3K27me3) and gene repression, we did not observe an association between EZH2 expression and the abundance of H3K27me3 by IHC studies in our clinical NKTL samples (supplemental Figure 3C). Interestingly, a lack of association between EZH2 and H3K27me3 has also been described in breast tumor subtypes[25,26] and in ovarian and pancreatic cancers.[26] This finding raises the possibility that EZH2 may have functions other than its activity on H3K27me3 in cancers, including NKTL. To investigate this possibility, we compared the ability of EZH2 wild-type (WT) and an EZH2 SET domain deletion mutant (EZH2 SETΔ) to increase the cell growth of NKTL cells. Interestingly, EZH2 SETΔ, which lacked the methyltransferase activity for H3K27me3, was still able to strongly promote cell growth of NKYS cells. This effect was as potent as EZH2 WT, as indicated by a similar increase in the percentage of GFP(+) cells with time (supplemental Figure 4), and increase in cell growth as measured by the MTS assay (Figure 3C). Both western blot (Figure 3D) and quantitative reverse-transcription PCR (qRT-PCR) analysis using a pair of primers that specifically amplifies the SET domain (supplemental Figure 5) confirmed the ectopic expression of EZH2 SETΔ in transfected cells. The ability of EZH2 SETΔ to deplete the H3K27me3 was also validated (Figure 3D; supplemental Figure 6C). These results indicate that the proproliferative property of EZH2 in NKTL is not mediated by its histone methyltransferase activity.

EZH2 directly activates CCND1 transcription by binding to its promoter independent of its methyltransferase activity in NKTL

To better understand how EZH2 promotes proliferation in NK cell lines, we explored the mechanism by which EZH2 regulates cell cycle genes. The study by Bracken and colleagues showed that suppression of EZH2 by RNA interference (RNAi) significantly decreased positive regulators of cell proliferation such as G1/*S*-cyclins,[27] so it is tempting to speculate that EZH2 directly regulates the transcription of these genes by binding to their genomic locus. The CCND1 transcript is reported to be upregulated in NKTL tissues compared with normal NK cells,[28] and high expression of CCND1 correlates with poor prognosis and decreased survival duration in NKTL.[29] Therefore, we examined whether the transcription of CCND1 is affected by EZH2 overexpression. Consistent with our findings on cell growth, qRT-PCR indicated that CCND1 mRNA levels increased substantially after EZH2 overexpression in NKYS (Figure 4A). Higher induction of CCND1 by EZH2-SETΔ could be explained by a previous study that ectopic EZH2 SETΔ depletes endogenous EZH2 and consistently displays higher levels of protein accumulation compared with the ectopic EZH2 WT.[30]

Next, we evaluated whether EZH2 can activate the activity of the CCND1 promoter in NKYS cells. Cotransfection of the EZH2 WT expression vector with the pGL4-CCND1-Luc reporter resulted in considerable activation of CCND1 promoter activity (Figure 4B). Consistent with prior results, activation of luciferase activity was also observed in cells transfected with EZH2 SETΔ (Figure 4B). Collectively, these results indicate that EZH2 positively regulates CCND1 transcription independent of its histone methyltransferase activity.

We then addressed whether EZH2 binds to the CCND1 promoter using ChIP-qPCR assays. Six pairs of primers, located sequentially along the proximal promoter, first exon, and intron 1 of CCND1 were used to quantify the ChIP-enriched DNA by real-time PCR (Figure 4C). A peak representing EZH2 binding was observed (~33-fold above background) at a region very close to the transcriptional start site of CCND1 (Figure 4D). ChIP using a control IgG showed no significant enrichment over the entire surveyed region (Figure 4D). By performing ChIP assays using a His-Tag antibody in NKYS transfected with His-Tagged EZH2 SETΔ, we showed that ectopically expressing EZH2 SETΔ resulted in significant enrichment of EZH2-DNA complexes, which was even higher than EZH2 WT (Figure 4E). This effect is specific to the SET domain, as EZH2 SANT domain deletion mutants abolished EZH2 transcriptional activity on the CCND1 promoter (Figure 4F). Furthermore, data from tumor samples that CCND1 mRNA levels correlate well with EZH2 mRNA levels are consistent with this finding (Figure 4G). Consistently, western blot analyses showed that CCND1 protein is expressed together with EZH2 in NK cell lines but not in normal NK cells (Figure 4H). Taken together, our findings identify CCND1 as a bona fide direct target of EZH2 in NKTL. Importantly, EZH2 acts as a transcriptional activator for the CCND1 gene without requiring histone methylation catalytic activity, which provides a mechanistic explanation for the proproliferative role of EZH2 SETΔ in NKTL.

Growth inhibition on depletion of endogenous EZH2 can be rescued by exogenous EZH2 SET mutants

Given that EZH2 is of functional importance in NKTL raises the possibility that targeting EZH2 may be a feasible strategy in NKTL. We first investigated the effects of depleting EZH2 on cell growth. Using 3 different short hairpin RNAs (shRNAs) targeting the EZH2 gene (Figure 5D; supplemental Figure 7A) in NKYS, we showed that depletion of EZH2 resulted in a substantial decrease in cell numbers, as revealed by the percentage of GFP+ cells (Figure 5A), and a specific concomitant decrease of CCND1 expression but not in other gene transcripts such as PRDM1 and IGF1 (Figure 5B; supplemental Figure 8). This result strengthens the postulation that EZH2 is required for expression of the proliferative gene CCND1 and suggests that downregulation of CCND1 is responsible for the reduction in cell growth in NKTL cells after EZH2 depletion.

Next, we sought to clarify if the reduction in cell growth is dependent on the methyltransferase activity of EZH2. Because EZH2 SETΔ is immune to EZH2 shRNA-2, which targets the SET domain, EZH2 shRNA-2 only depleted endogenous WT EZH2 but not the EZH2 SETΔ after being introduced into the cells, as expected (supplemental Figure 7B). Indeed, EZH2 SETΔ was able to prevent the reduction in cell numbers mediated by EZH2 shRNA-2, whereas reintroduction of EZH2 WT could not (Figure 5C, left). These rescue experiments excluded the possibility that the cell death phenotype occurred because of an off-target effect of EZH2 shRNA and, at the same time, confirming that the prosurvival effect of endogenous EZH2 does not require its enzymatic activity. Similar results were obtained in KHYG1 (Figure 5C, right), another NKTL cell line, indicating a consistent requirement for expression of EZH2 in the growth and survival of NK tumor cells.

Inhibition of EZH2 by 3-deazaneplanocin A (DZNep) induced growth inhibition and apoptosis of malignant NK cell lines

The effects seen with EZH2 knockdown suggest that EZH2 may be a therapeutic target in NKTL. We next explored the use of a

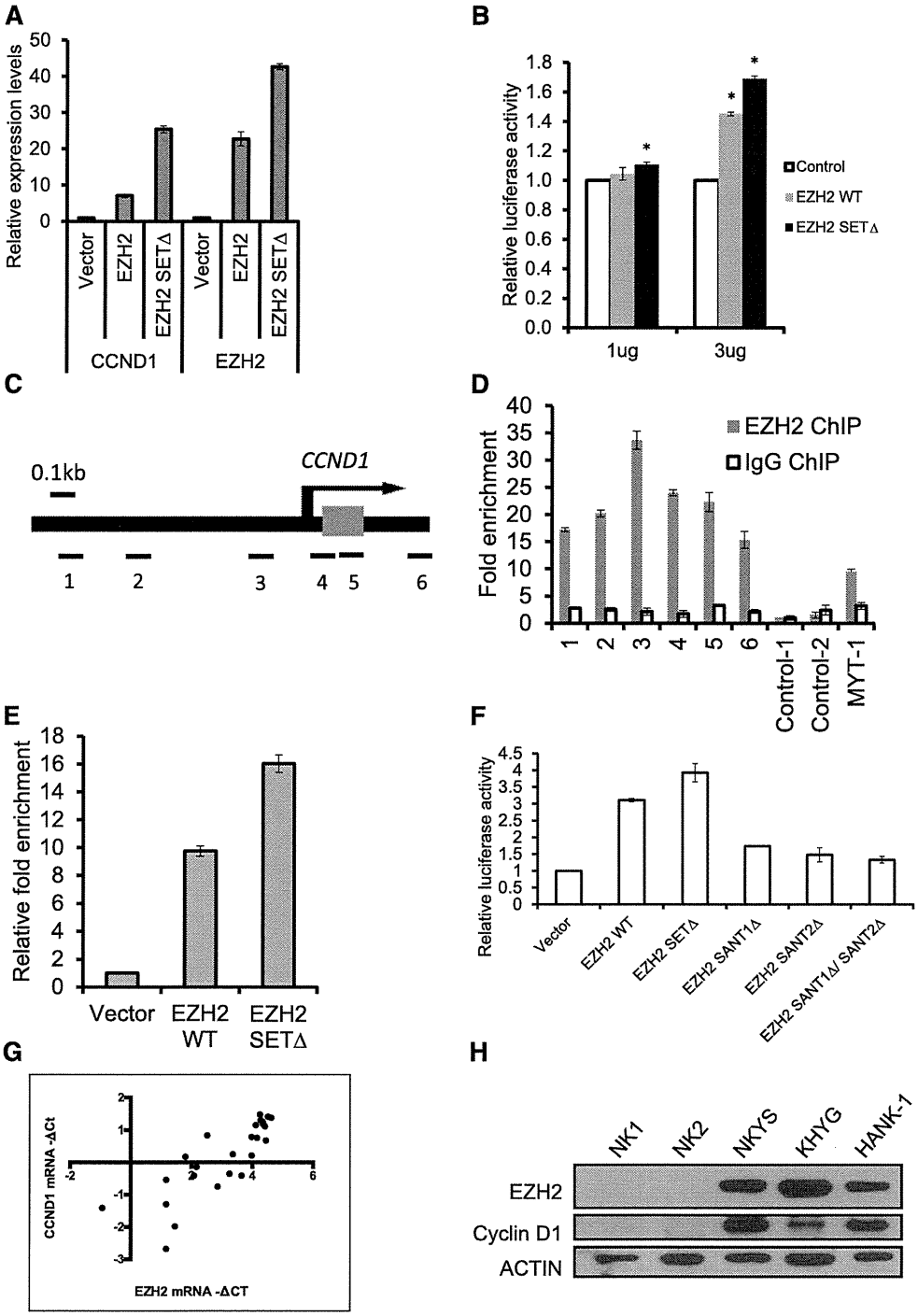

Figure 4. EZH2 positively regulates CCND1 transcription by binding to its promoter in NKTL cells. (A) Overexpression of EZH2 induces the expression of CCND1. Vectors expressing EZH2 (pcDNA-EZH2 or pcDNA-EZH2 SETΔ) were transiently transfected into NKYS cells. The RNA harvested from the cells at 24 hours after transfection was isolated, reverse-transcribed, subjected to qPCR by using primers specific for CCND1 mRNA, and normalized with GAPDH. (B) Luciferase promoter assay showing that EZH2 activates CCND1 transcription. NKYS cells were transfected with the luciferase reporter construct pGL4 containing the CCND1 promoter and various amounts of EZH2 WT/SETΔ plasmid or a control vector. Luciferase activities were measured after 24 hours. Luciferase readings were further normalized to the internal control pRL null. Results are presented as averages of triplicate experiments. Error bars represent standard deviation. * denotes $P < .01$ with respect to cells transfected with the same amount of control vector. (C) Genomic structure of human CCND1. The locations of the 6 pairs of primer sets used to detect the ChIP-enriched DNA fragments are indicated. (D) ChIP-qPCR for endogenous EZH2 binding to the CCND1 gene. ChIP assays were performed by using NKYS. Real-time PCR was performed with immunoprecipitated chromatin fragments obtained by using an anti-EZH2 antibody or an irrelevant antibody (IgG) as a control. A known EZH2 binding site in the promoter region of the MYT-1 gene was amplified as a positive control for the ChIP assays. (E) ChIP-qPCR for ectopically expressed EZH2 WT and EZH2 SETΔ binding to the CCND1 gene. ChIP assays were performed by using NKYS transfected by a pcDNA4.1/Myc-His vector or a plasmid expressing EZH2 WT and EZH2-SETΔ. Real-time PCR was performed with immunoprecipitated chromatin fragments obtained by using an anti-His antibody. Primer set 3, which amplifies a region representing EZH2 binding, was used to detect the ChIP-enriched DNA fragments. (F) Luciferase promoter assay showing the inability of EZH2 SANT domain deletion mutants to activate CCND1 transcription. NKYS were transfected with 3μg of EZH2 WT/SETΔ/SANTΔ plasmids or a control vector. Luciferase activities were measured after 24 hours. (G) Correlation between mRNA levels for EZH2 and CCND1 determined by qRT-PCR in NKTL clinical samples. Spearman correlation coefficient = 0.8608; $P < .0001$. (H) Western blot analysis of protein levels of CCND1 and EZH2 in NK cell lines and normal NK cells.